Correspondence to:

S.-H. Zhang,
tozhangshuanhong@163.com

An Unusually Warm Upper-Crust in the Late Paleozoic North China Continental Arc: Implications for the Thermal Modification of the Giant Bayan Obo REE Deposit

Shuan-Hong Zhang[1,2] , **Mei-Fu Zhou[3]** , **Yue Zhao[1,2]**, **Qi-Qi Zhang[1,2]**, **Guo-Hui Hu[1,2]**, **Ling-Hao Kong[1,2]**, **Sen Wang[1,2]**, **Jun-Ling Pei[1,2]** , and **Daniel P. Miggins[4]**

[1]Institute of Geomechanics, Chinese Academy of Geological Sciences, MNR Key Laboratory of Paleomagnetism and Tectonic Reconstruction, Beijing, China, [2]Research Center of Polar Geosciences, China Geological Survey, Beijing, China, [3]Institute of Geochemistry, Chinese Academy of Sciences, Guiyang, China, [4]College of Earth, Ocean and Atmospheric Sciences, Oregon State University, Corvallis, OR, USA

Abstract The genesis and timing of formation of the giant Bayan Obo deposit, the world's largest rare earth element (REE) deposit in the western part of the late Paleozoic northern North China continental arc (NCA), are highly controversial due to complex mineral assemblages and reported ages of mineralization. We conducted new zircon U-Pb and $^{40}Ar/^{39}Ar$ dating of metamorphic and igneous Neoarchean to Permian mid-to upper-crustal rocks exhumed along a north−south corridor across the western NCA and its retroarc foreland. The results show that the mid- to upper-crust of the western part of the NCA has been strongly affected by thermal modifications during arc construction in the late Paleozoic, while the retroarc foreland remained thermally stable. Our results first reveal an unusually warm upper-crust around Bayan Obo during the late Paleozoic with high geothermal gradients of 50.0 ± 8.3 to 88.3 ± 8.3°C/km and strong thermal modification of the upper-crust during arc construction. This unusually warm upper-crust and high geothermal gradients resulted in intensive thermal perturbations and recrystallization of REE-bearing minerals in the Bayan Obo deposit, as well as formation of high-grade REE ores and complete or partial resetting (U-)Th-Pb isotopic systems of REE minerals. Our identification of the unusually warm upper-crust and high geothermal gradients in the western part of the NCA provides important constraints on genesis, timing and thermal modification of the giant Bayan Obo deposit, as well as other REE deposits with complex isotopic ages.

Plain Language Summary The Bayan Obo deposit is the largest rare earth element (REE) deposit in the world. Located in North China, its formation and timing of mineralization have been debated for over 60 years. We conducted thermochronometric investigations on metamorphic and igneous minerals (hornblende, muscovite and biotite) of the mid-to upper-crusal rocks around Bayan Obo and concluded that anomalously high geothermal gradients led to extensive crustal mobilization and enrichment of the REE minerals to form the ore deposits. We suggest that these thermal perturbation events were also responsible for resetting isotopic clocks (e.g., (U-)Th-Pb systems) of REE minerals, ultimately causing uncertainties in the mineralization ages of the Bayan Obo deposit and geological reconstructions of the region.

1. Introduction

The thermal state of the continental crust plays an important role in the understanding of the geophysical, geological, and geochemical evolution of continental magmatic arcs (Rothstein & Manning, 2003). The thermal state of the continental crust controls not only rheology and deformation which are sensitive to temperature, but also overprints of early formed ore deposits in mid- to upper-crustal levels. Modern continental arcs, such as the central Andes arc, have large crustal thicknesses of 50–80 km (Beck et al., 1996; McGlashan et al., 2008) and are therefore characterized by low average geothermal gradients (ca. 15°C/km) by using a crustal thickness of 60 km and Moho temperature of 900°C (Cao et al., 2019). However, the mid-to upper-crust may have high geothermal gradients of 30–50°C/km as a result of heat transfer due to magma migration in continental arcs (Cao et al., 2019; Rothstein & Manning, 2003). Numerical modeling results show that geothermal gradients in the upper-crust in continental arcs are high but decrease significantly in the lower crust below the level at which magmas pond (Rothstein & Manning, 2003). Extremely high geothermal gradients >60°C/km have been reported in the upper-crust of some low-pressure/high-temperature metamorphic belts including magmatic arcs, regions of

Investigation: Shuan-Hong Zhang, Yue Zhao, Qi-Qi Zhang, Guo-Hui Hu, Jun-Ling Pei
Methodology: Shuan-Hong Zhang
Project Administration: Shuan-Hong Zhang
Resources: Shuan-Hong Zhang
Software: Daniel P. Miggins
Validation: Shuan-Hong Zhang
Visualization: Shuan-Hong Zhang
Writing – original draft: Shuan-Hong Zhang
Writing – review & editing: Shuan-Hong Zhang, Mei-Fu Zhou, Yue Zhao, Jun-Ling Pei

extension, regions of thickened crust in continent-continent collision zones and accretionary wedges (De Yoreo et al., 1991; Wickham, 1987), and the large magmatic fluxes associated with the formation of magmatic arcs were considered to provide an adequate heat source for low-pressure metamorphism and high geothermal gradients (De Yoreo et al., 1991).

The northern margin of the North China Craton (NCC) was a continental magmatic arc (northern North China continental arc, NCA) during the late Paleozoic and is marked by abundant Carboniferous-Permian dioritic-granitic batholiths or plutons due to the southward subduction of the Paleo-Asian Ocean (Cope, 2017 and references therein; S. H. Zhang et al., 2007, 2009; Figure 1). Previous studies of a north−south corridor across the middle part of the NCA and retroarc foreland (Figure 1) indicate that the mid- to upper-crust of the arc was strongly heated (presumably because of magma advection) during the late Paleozoic with high average paleogeo-thermal gradients of 37.0–44.5°C/km. In contrast, the mid- to upper-crust beneath the retroarc foreland remained cold with low paleogeothermal gradients (S. H. Zhang et al., 2019). However, it is still uncertain whether the mid-to upper-crust of the western part of the NCA was strongly heated during the late Paleozoic.

Bayan Obo, the world's largest rare earth element (REE) deposit is located in the western part of the NCA and is hosted within carbonatite sills/dykes that emplaced into Mesoproterozoic sedimentary rocks of the Bayan Obo Group (Figure 2, S. H. Zhang, Zhao, Liu, et al., 2017). Although the primary REE mineralization in the Bayan Obo deposit was mostly thought to be related to the 1.32−1.30 Ga carbonatitic magmatism (Chen et al., 2020; Fan et al., 2016; Le Bas et al., 2007; Q. Li et al., 2018; K. F. Yang et al., 2019; S. H. Zhang, Zhao, Liu, et al., 2017; Zhu et al., 2015), monazite and bastnäsite (dominant REE-bearing minerals of the Bayan Obo deposit) have highly variable $^{208}Pb/^{232}Th$ ages ranging from ca. 1,320 to ca. 260 Ma (X.-C. Li et al., 2021, 2022; Ling et al., 2013; Song et al., 2018; Wei et al., 2022; K. F. Yang et al., 2019; Y. H. Yang et al., 2019). This large spread in ages resulted in numerous interpretations about the genesis and timing of the REE mineralization in the Bayan Obo deposit (Campbell et al., 2014; Chao et al., 1997; Le Bas et al., 2007; Smith et al., 2015; X. Y. Yang et al., 2017).

In this contribution, we present new zircon U-Pb and hornblende, muscovite and biotite $^{40}Ar/^{39}Ar$ ages of the Archean-Paleoproterozoic basement complexes, Mesoproterozoic-Silurian slates/schists and Permian granites from a north−south corridor. Samples were taken along a cross-section from Bayan Obo to Baotou across the western NCA and the retroarc foreland. Our data add information in regards to the thermal state of the mid-to upper-crust of the NCA, in relation to the genesis of the Bayan Obo deposit.

2. Geological Setting and Samples

The NCA extends for over 1,600 km with emplacement of large volumes of late Carboniferous-Permian plutons composed mainly of diorite, granite, tonalite and gabbro (Figure 1). There are also several Devonian alkaline and mafic intrusions and large volumes of latest Permian-Triassic plutons consisting mainly of granite and gabbros (Figure 2). Jurassic to Cretaceous intrusive and volcanic rocks are common in the middle and eastern parts of the NCA due to the westward subduction of the Paleo-Pacific Plate beneath the eastern margin of the Eurasian continent and decratonization of the NCC (J. H. Yang et al., 2008; S. H. Zhang, Zhao, Davies, et al., 2014). Thermobarometrical data and deformation styles show that the middle part of the NCA was deeply exhumed and eroded with exposure of mid-crustal plutonic and Archean-Paleoproterozoic basement complexes and absences of the Mesoproterozoic to Permian sedimentary and volcanic successions in many areas (S. H. Zhang et al., 2007; S. H. Zhang & Zhao, 2013).

In contrast, the western part of the NCA was relatively weakly exhumed and eroded, and the Meso-Neoproterozoic sedimentary and Permian volcanic and sedimentary successions are preserved in many places along the arc (Figure 2). Late Carboniferous-Permian arc plutons are common in this area with emplacement of some Devo-nian alkaline intrusions and large Triassic granite and alkaline intrusions. Emplacement depths of the Permian plutons in this area estimated by hornblende-plagioclase thermobarometry range from ca. 15 to ca. 6 km (Wu et al., 2014; S. H. Zhang & Zhao, 2017), indicating the emplacement of these plutons in mid-to upper-crustal levels. The emplacement depths of the Permian plutons increase from north to south (S. H. Zhang & Zhao, 2017), consistent with existence of Permian volcanic and sedimentary successions around Bayan Obo in the north-ern part of the NCA (Jia et al., 2003; S. H. Zhang et al., 2016) and lack of Permian volcanic and sedimentary successions around Guyang in the southern part of the NCA (Figure 2). Thermochronometric investigations on these exhumed upper-crustal rocks of different ages can provide new insights into the thermal state of the mid-to
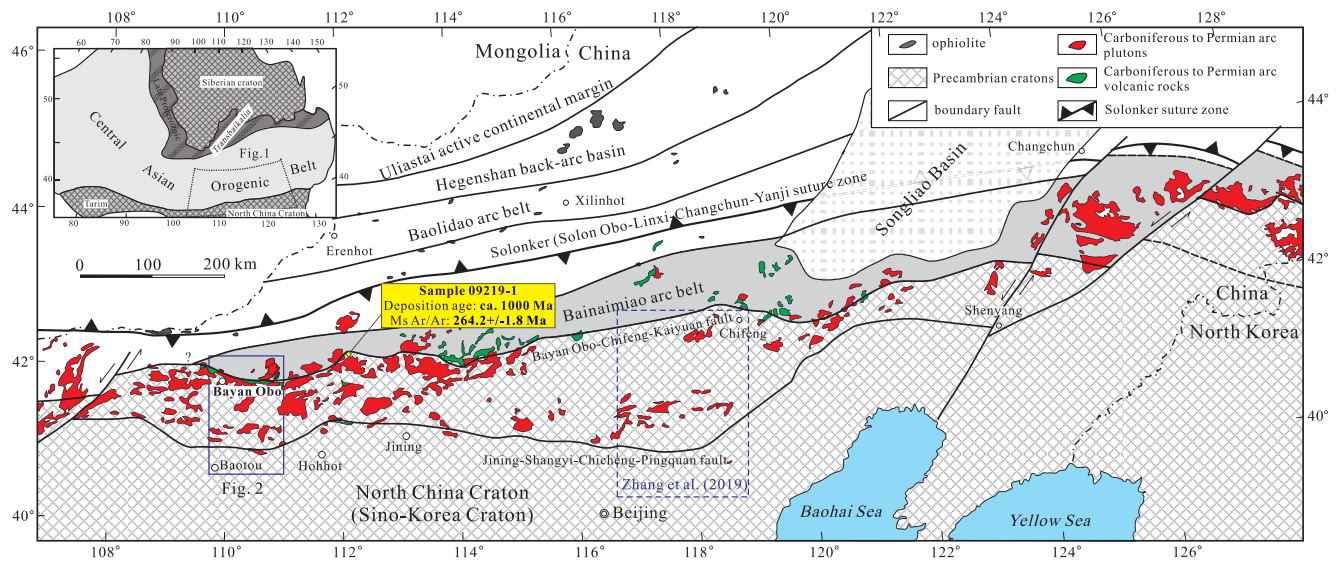
Figure 1. Sketch tectonic map of the southern Central Asian orogenic belt and the northern North China Craton showing distributions of the Carboniferous to Permian arc volcanic and intrusive rocks in the NCA (modified from S. H. Zhang, Zhao, Ye, et al. (2014)). Locations of sample 09219-1 and the north−south corridor from Weichang to Zunhua investigated by S. H. Zhang et al. (2019) are shown in the map.

upper-crust and thermal modifications of ore deposits in this area. However, thermochronometric studies of the basement complexes and arc plutons in the western part of the NCA have not been performed till present.
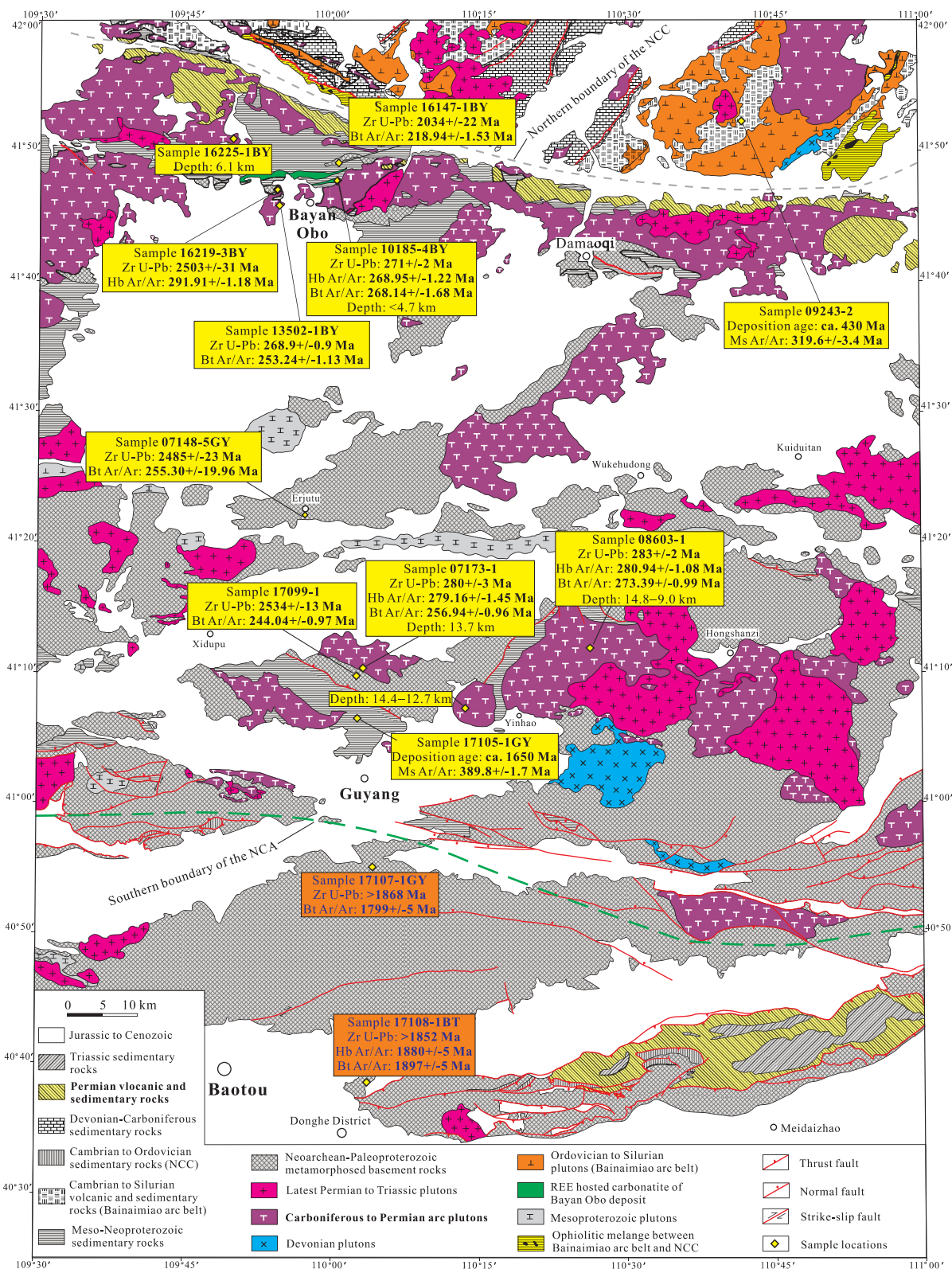
The retroarc foreland in the western part of the NCA is characterized by abundant Neoarchean to Paleoproterozoic metamorphic basement complexes (Figure 2). Although there are no late Paleozoic magmatic rocks in these areas, Triassic granitic and alkaline plutons are common and intrude the basement complexes (Figure 2). Since the exhumation of the basement complexes occurred during the Mesozoic and the cover sequence is Meso-Neoproterozoic to Permian sedimentary succession of ca. 5 km thick (Jia et al., 2003; Z. H. Liu et al., 2003), the basement complexes were likely to be exhumed from the upper-crustal levels of >5.0 km. Thermochronometric studies of these basement complexes can be used to constrain the thermal state of the upper-crust of the retroarc foreland during the construction of the NCA.

Thirteen samples for thermochronometric investigations were collected from a north−south corridor from Bayan Obo to Baotou across the western part of the NCA and the retroarc foreland (Figures 1 and 2). Among these, four samples are from Neoarchean to Paleoproterozoic metamorphic basement complexes (16219-3BY, 16147-1BY, 07148-5GY, and 17099-1GY) in the NCA, five samples are from the late Carboniferous-Permian pluton (10185-4BY, 16225-1BY, 13502-1BY, 07173-1, and 08603-1) in the NCA, two samples are from the Silurian and Mesoproterozoic quartz schists (samples 09219-1, 09243-2) in the northern margin of the NCA, one sample is from the Mesoproterozoic slate (17105-1GY) in the southern margin of the NCA and two samples are from the Neoarchean to Paleoproterozoic metamorphic basement rocks (17107-1GY and 17108-1BT) south to the NCA. Four samples (16219-3BY, 16147-1BY, 10185-4BY, 16225-1BY, and 13502-1BY) were collected from or near the Bayan Obo deposit. Locations and descriptions of all the samples are listed in Table 1. A detailed description of the samples is listed in Text S1 in Supporting Information S1. Representative photomicrographs of all the samples are shown in Figure 3 and Figure S1 in Supporting Information S1.

3. Methods

3.1. Analytical Methods

Electron microprobe analyses on plagioclase and hornblende were performed at the Wuhan Sample Solution Analytical Technology Company Limited, Hubei Province. Zircon LA-ICP-MS dating and trace element analyses were conducted at the Wuhan Sample Solution Analytical Technology Company Limited, Hubei Province and the Key Laboratory of Paleomagnetism and Tectonic Reconstruction of Ministry of Natural Resources, Institute of Geomechanics, Chinese Academy of Geological Sciences (CAGS) in Beijing. ^{40}Ar/^{39}Ar incremental heating

Figure 2. Geological map of the northern North China Craton across the western part of the NCA and the retroarc foreland showing new obtained zircon U-Pb and $^{40}Ar/^{39}Ar$ ages and emplacement depth of Permian granitic plutons (modified from Jia et al. (2003) and Z. H. Liu et al. (2003)).

Table 1
Locations and Descriptions of Samples Across the Western Part of the NCA and the Retroarc Foreland

Sample no.	Longitude (E)	Latitude (N)	Rock type	Mineral assemble (volume percentage)	Location	Zircon U-Pb ages and references
Neoarchean to Paleoproterozoic metamorphic basement rocks in the NCA						
16219-3BY	109°54.4′	41°47.0′	Granitic gneiss	Kf (50%) + Q (25%) + Pl (20%) + Hb (5%)	Bayan Obo	2,528 ± 32 Ma (This study)
16147-1BY	110°00.4′	41°49.0′	Granitic gneiss	Q (35%) + Kf (20%) + Ms (30%) + Pl (5%) + Bt (5%) + Ch (5%)	Bayan Obo	2,017 ± 34 Ma (This study)
07148-5GY	109°56.9′	41°22.2′	Granitic gneiss	Kf (55%) + Pl (20%) + Q (20%) + Bt (3%) + Ep (2%)	Hejiao	2,485 ± 23 Ma (This study)
17099-1GY	110°02.6′	41°09.9′	Granitic gneiss	Kf (40%) + Q (25%) + Pl (7%) + Bt (25%) + Ep (3%)	Guyang	2,552 ± 22 Ma (This study)
Late Carboniferous-Permian pluton in the NCA						
10185-4BY	110°00.2′	41°47.8′	Granite	Kf (60%) + Q (20%) + Pl (13%) + Hb (4%) + Bt (3%)	East Bayan Obo pluton	271 ± 2 Ma (This study)
16225-1BY	109°49.8′	41°50.8′	Quartz diorite	Pl (55%) + Kf (15%) + Hb (10%–15%) + Q (10%) + Bt (5%–10%)	West Bayan Obo pluton	270 ± 2 Ma
13502-1BY	109°54.5′	41°45.9′	Gneissic granite	Kf (50%) + Q (25%) + Pl (20%) + Bt (5%)	South Bayan Obo pluton	268.8 ± 1.2 Ma (This study)
07173-1	110°03.0′	41°10.4′	Quartz diorite	Pl (65%) + Kf (15%) + Bt (10%) + Hb (5%–10%) + Q (5%–10%)	Rentaihe pluton	280 ± 3 Ma (S. H. Zhang & Zhao, 2017)
08603-1	110°26.4′	41°11.8′	Quartz diorite	Pl (60%) + Bt (10%–15%) + Hb (10%) + Kf (10%) + Q (5%–10%)	Yinhao pluton	283 ± 2 Ma (S. H. Zhang & Zhao, 2017)
Mesoproterozoic and Silurian schist in the northern edge of NCA						
09219-1	112°10.3′	42°06.0′	Quartz schist (metamorphosed from quartz sandstone of the Mesoproterozoic Bayan Obo Group)	Q (70%) + Ms (20%) + Bt (5%) + Kf (4%) + Pl (1%)	North Siziwangqi	Ca. 1,000 Ma
09243-2	110°42.0′	41°52.3′	Quartz schist (metamorphosed from the Silurian sandstone)	Q (50%) + Ms (15%) + Kf (15%) + Ser (14%) + Pl (5%) + Grt (1%)	Northeast Damaoqi	Ca. 430 Ma (S. H. Zhang, Zhao, Ye, et al., 2014)
Mesoproterozoic slate in the southern edge of NCA						
17105-1GY	110°02.6′	41°06.5′	Calcite-rich slate (Mesoproterozoic Agulugou Formation)	Cal (55%) + Q (20%) + Ms (15%) + Fsp (10%)	North Guyang	Ca. 1,650 Ma
Neoarchean to Paleoproterozoic metamorphic basement rocks south to the NCA (retroarc foreland)						
17107-1GY	110°04.1′	40°55.0′	Biotite-plagioclase gneiss	Pl (45%) + Q (20%) + Px (15%) + Hb (10%) + Bt (5%) + Kf (5%)	South Guyang	2,500−1,880 Ma (This study)
17108-1BT	110°03.5′	40°38.5′	Biotite-plagioclase gneiss	Pl (55%) + Kf (15%) + Q (15%) + Hb (8%) + Px (4%) + Bt (3%)	East Baotou	2,809−1,920 Ma (This study)

Note. Mineral abbreviations: Pl, plagioclase; Bt, biotite; Hb, hornblende; Kf, K-feldspar; Q, quartz; Px, pyroxene; Ms, muscovite; Grt, garnet; Chl, chlorite; Ep, epidote; Cal, calcite; Ser, sericite; Fsp, feldspar.

analysis of 15 hornblende, muscovite and biotite samples was performed in Oregon State University (OSU) Argon Geochronology Laboratory, USA. Two muscovite samples were analyzed at the Laboratory of Isotope Thermochronology, Institute of Geology, CAGS, Beijing. Detailed operating conditions for laboratory procedures and data reduction are listed in Text S2 in Supporting Information S1. The sizes of hornblende, muscovite and biotite samples for $^{40}Ar/^{39}Ar$ dating are 250–600 µm.
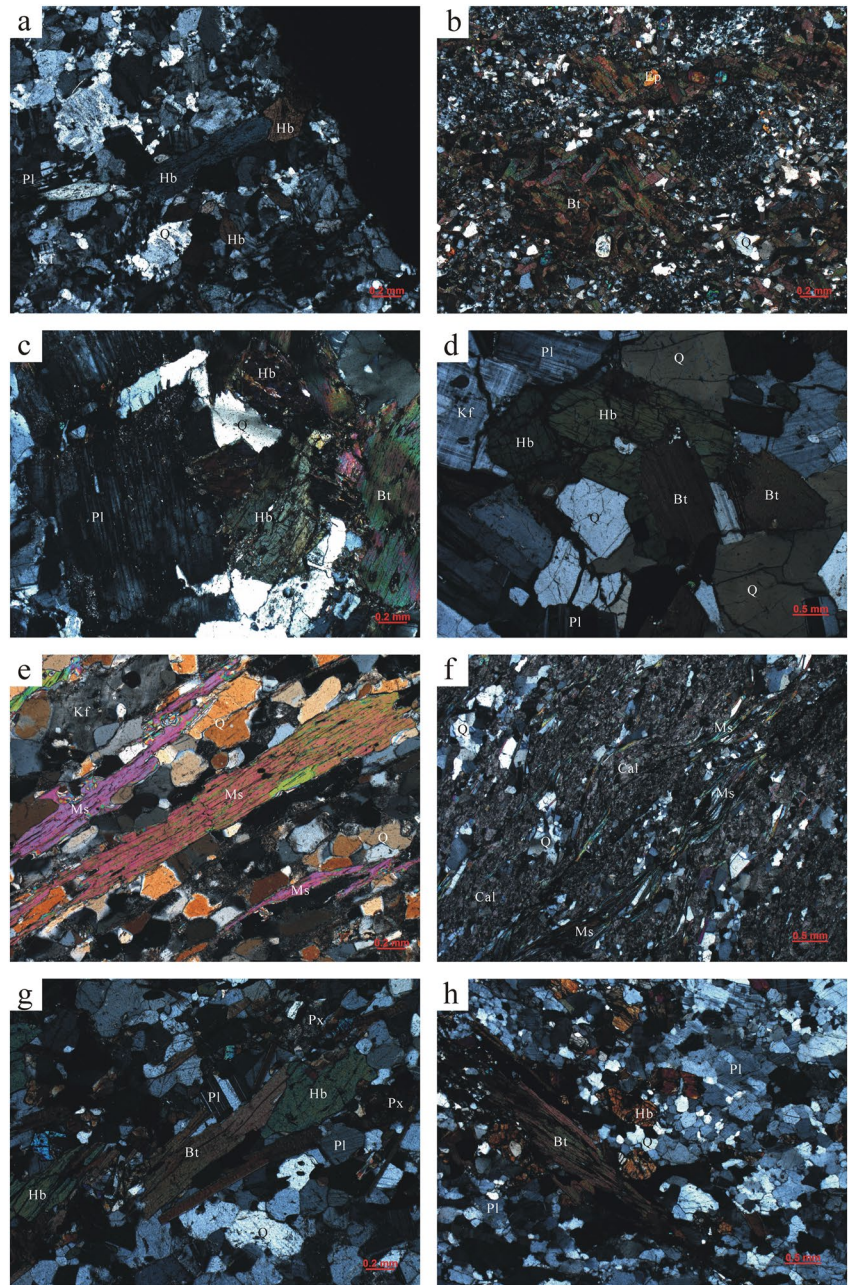
Figure 3. Photomicrographs of representative samples (plane polarized light) for U-Pb and $^{40}Ar/^{39}Ar$ dating. (a) Sample 16219-3BY; (b) sample 17099-1GY; (c) sample 16225-1BY; (d) sample 08603-1; (e) sample 09243-2; (f) sample 17105-1GY; (g) sample 17107-1GY; (h), sample 17108-1BT. Mineral abbreviations: Pl, plagioclase; Bt, biotite; Hb, hornblende; Kf, K-feldspar; Q, quartz; Px, pyroxene; Ms, muscovite; Ep, epidote; Cal, calcite.

3.2. Geothermobarometry

Hornblende-plagioclase thermobarometry has been widely used to estimate the crystallization $P–T$ conditions of granitic plutons with mineral assemblage of plagioclase, hornblende, K-feldspar, quartz, biotite, titanite, and magnetite (e.g., Ague, 1997; Anderson et al., 2008; Anderson & Smith, 1995; Jagoutz, 2014; Jagoutz et al., 2013; Johnson & Rutherford, 1989; Mutch et al., 2016; Schmidt, 1992; Stein & Dietl, 2001). We used the Al-in-hornblende barometer calibration proposed by Mutch et al. (2016) since this calibration was based on new experimental data on the composition of magmatic amphiboles synthesized from a variety of granite bulk compositions at near-solidus temperatures and wide pressures of 0.8–10 kbar and can be used for granitoids emplaced in shallow crustal depths (≤4 km). As shown in Table 2 and Table S3, the crystallization pressures of

Table 2
Al-In-Hornblende Geothermobarometric Data of the Permian Granitoids Near Bayan Obo Deposit

Analytical spots	Plag Ab(%)	Plag An(%)	Amph Al(Total)	T(ed–tr) (°C)	T(ed–ri) (°C)	P–J&R (kbar)	P–Sch (kbar)	P–A&S (kbar)	P–Mu (kbar)	Paver (kbar)
16225-1BY (quartz diorite)										
1-1	86.4	13.1	1.095	624	637	1.17	2.20	2.37	**2.05**	**1.89**
1-2	72.4	26.9	1.053	645	645	0.99	2.00	2.14	**1.95**	
1-3	72.3	27.0	0.291	Not suitable for Al-in-hornblende geobarometer						
1-4	71.9	27.5	0.243	Not suitable for Al-in-hornblende geobarometer						
1-5	71.7	27.6	0.426	Not suitable for Al-in-hornblende geobarometer						
2-1	78.2	21.2	1.097	691	671	1.18	2.21	2.24	**2.06**	
2-2	84.0	15.4	1.163	653	579	1.46	2.53	2.65	**2.23**	
2-3	72.6	26.9	1.113	694	692	1.25	2.29	2.15	**2.10**	
2-4	69.5	30.0	1.096	673	677	1.18	2.21	2.20	**2.06**	
2-5	88.0	11.6	1.149	650	596	1.40	2.46	2.64	**2.19**	
3-1	60.1	39.4	1.064	696	713	1.04	2.06	1.72	**1.98**	
3-2	74.6	24.6	1.023	641	628	0.87	1.86	2.02	**1.88**	
3-3	68.9	30.5	1.061	632	661	1.03	2.04	2.12	**1.97**	
3-4	74.3	24.8	1.136	677	678	1.34	2.40	2.37	**2.16**	
3-5	59.7	39.6	1.090	721	710	1.15	2.18	1.86	**2.04**	
4-1	81.6	17.6	0.823	601	582	0.02	0.91	0.85	**1.45**	
4-2	74.7	24.6	0.742	597	610		0.52	0.56	**1.29**	
4-3	75.4	23.9	0.819	618	615	0.00	0.89	0.97	**1.44**	
4-4	74.7	24.5	0.982	619	624	0.69	1.66	1.81	**1.78**	
4-5	75.5	23.6	0.851	620	604	0.14	1.04	1.10	**1.50**	
10185-4BY (granite)										
1-1	92.3	6.8	1.448	758	644	2.67	3.88	4.10	**3.07**	**2.87**
1-2	91.4	8.0	1.403	724	649	2.48	3.67	3.85	**2.92**	
1-3	90.9	8.0	1.477	706	658	2.79	4.02	4.16	**3.16**	
1-4	90.7	8.2	1.395	738	662	2.44	3.63	3.74	**2.90**	
1-5	91.1	8.1	1.420	750	673	2.55	3.75	3.77	**2.98**	
2-1	89.8	9.5	1.345	747	652	2.23	3.39	3.55	**2.74**	
2-2	89.6	9.9	1.386	803	671	2.40	3.59	3.63	**2.87**	
2-3	87.7	11.8	1.380	821	672	2.38	3.56	3.58	**2.85**	
2-4	89.2	10.1	1.380	785	678	2.38	3.56	3.53	**2.85**	
2–5	88.7	10.9	0.451	Not suitable for Al-in-hornblende geobarometer						
3-1	93.5	5.9	1.352	752	609	2.26	3.42	3.71	**2.76**	
3-2	91.5	7.7	1.354	765	643	2.27	3.44	3.64	**2.77**	
3-3	92.1	7.3	1.306	722	619	2.06	3.20	3.47	**2.63**	
3-4	92.2	7.1	1.400	771	645	2.46	3.66	3.86	**2.91**	
3-5	93.1	6.2	1.316	768	649	2.11	3.25	3.42	**2.66**	
4-1	89.7	9.2	1.418	800	678	2.54	3.74	3.71	**2.97**	
4-2	90.1	9.3	1.353	769	679	2.26	3.43	3.40	**2.77**	
4-3	89.6	10.0	1.384	781	681	2.39	3.58	3.52	**2.86**	

Table 2
Continued

Analytical spots	Plag Ab(%)	Plag An(%)	Amph Al(Total)	T(ed–tr) (°C)	T(ed–ri) (°C)	P–J&R (kbar)	P–Sch (kbar)	P–A&S (kbar)	P–Mu (kbar)	Paver (kbar)
4-4	88.7	10.6	1.432	782	705	2.60	3.80	3.48	**3.01**	
4-5	95.7	3.6	1.389	786	608	2.42	3.60	3.90	**2.88**	

Note. Plag Ab—the atomic ratio [Na/(Na + Ca + K)]; Plag An—the atomic ratio [Ca/(Na + Ca + K)]; Amph Al (Total)—the total number of Al cations calculated in the structural formula of hornblende (Table S1); T(ed–tr)—temperature calculated using plagioclase–hornblende geothermometer A (edenite–tremolite) of Holland and Blundy (1994); T(ed–ri)—temperature calculated using plagioclase–hornblende geothermometer B (edenite–richterite) of Holland and Blundy (1994); P–A&S—the temperature–corrected pressure, calculated using Anderson and Smith (1995); P–J&R—pressure calculated using Johnson and Rutherford (1989); P–Sch—pressure calculated using Schmidt (1992); P–Mu—pressure calculated using Mutch et al. (2016); Paver—average crystallization pressure of Mutch et al. (2016). The bold values in Table 2 are crystallization pressures being used in this study.

the same pluton obtained by the calibration from Mutch et al. (2016) are more stable than those obtained by other calibrations (Anderson & Smith, 1995; Johnson & Rutherford, 1989; Schmidt, 1992), indicating the reliability of this calibration than others. Closure temperatures for zircon U-Pb and hornblende, biotite and muscovite Ar/Ar isotopes are compiled from Chew and Spikings (2015), Gehrels et al. (2003), Hodges (2014), McDougall and Harrison (1999), Nadin et al. (2016), and Saleeby et al. (2007).

4. Results

4.1. Plagioclase and Hornblende Compositions and Crystallization Pressures

Electron microprobe analytical results of hornblende and plagioclase from two Permian plutons near Bayan Obo deposit are listed in Tables S1 and S2, respectively. According to the nomenclature of Leake et al. (1997), hornblende from sample 10185-4BY is classified as ferroedenite, ferrohornblende and ferroactinolite, and that from sample 16225-1BY is classified as magnesiohornblende and actinolite. Plagioclase from sample 10185-4BY is classified as albite and oligoclase with An numbers (the percent atomic ratio [Ca/(Na + Ca + K)]) ranging from 3.6 to 10.9; that from sample 16225-1BY is classified as oligoclase and andesine with An numbers ranging from 11.6 to 39.6.

Most hornblendes from sample 16225-1BY have Fe/(Fe + Mg) ratios ranging from 0.463 to 0.538, which is within the recommended range (0.40–0.65) for hornblende barometry (Anderson & Smith, 1995). The An numbers of most plagioclase (70%) from sample 16225-1BY are similar to the recommended An numbers of 25–35 for plagioclase coexisting with hornblende for hornblende-plagioclase thermobarometry (Stein & Dietl, 2001). Calibration of the Al-in-hornblende barometer on sample 16225-1BY yields an average crystallization pressure of 1.89 kbar (Table 2), corresponding to an emplacement depth of 6.1 km (1 kbar is ca. 3.25 km in depth, Stein & Dietl, 2001; S. H. Zhang & Zhao, 2017) for the Permian granitoid pluton northwest to the Bayan Obo deposit.

Hornblende from sample 10185-4BY from the East Bayan Obo granitic pluton has high Fe/(Fe + Mg) ratios of 0.710–0.801 and the average crystallization pressure obtained by Al-in-hornblende barometer is 2.87 kbar (Table 2). This Fe-rich hornblende (Fe/(Fe + Mg) ratios > 0.65) is crystallized in low-fO$_2$ granites (Anderson & Smith, 1995) and Al-in-hornblende barometer of this Fe-rich hornblende will yield pressures that are too high by a factor of two to three in comparison with pressures obtained from adjacent metamorphic assemblages (Anderson & Smith, 1995). Therefore, the crystalization pressure of 2.87 kbar obtained by Fe-rich hornblende is two to three times higher and the real crystallization pressure of sample 10185-4BY is less than 1.44 kbar (half of 2.87 kbar) and the emplacement depth of the East Bayan Obo granitic pluton is <4.7 km. This inferred emplacement depth is similar to that of the Permian granitoid pluton northwest to the Bayan Obo deposit and we use ca. 6.0 km as emplacement depths of the late Paleozoic plutons around the Bayan Obo deposit.

Using the new calibration from Mutch et al. (2016), the crystallization pressures of the Carboniferous-Permian arc plutons in the western part of the late Paleozoic NCA were recalculated by using the previously published plagioclase and hornblende composition data (Wu et al., 2014; S. H. Zhang & Zhao, 2017). The results are listed in Table S3 and the average crystallization pressures of the Carboniferous-Permian arc plutons in the western part of the late Paleozoic NCA range from 2.04 kbar (6.63 km in depth) to 4.54 kbar (14.76 km in depth). These

recalculated and new obtained geothermobarometric data (Table S3 and Table 2) are used for calculation of the paleogeothermal gradient in Section 5.3.

4.2. U-Pb Ages

Eight samples were selected for zircon U-Pb and trace element analyses and the results were listed in Table S4 and were plotted in Figures 4 and 5. Representative CL images of zircons are shown in Figures 4 and 5 and Figures S2−S9 in Supporting Information S1.

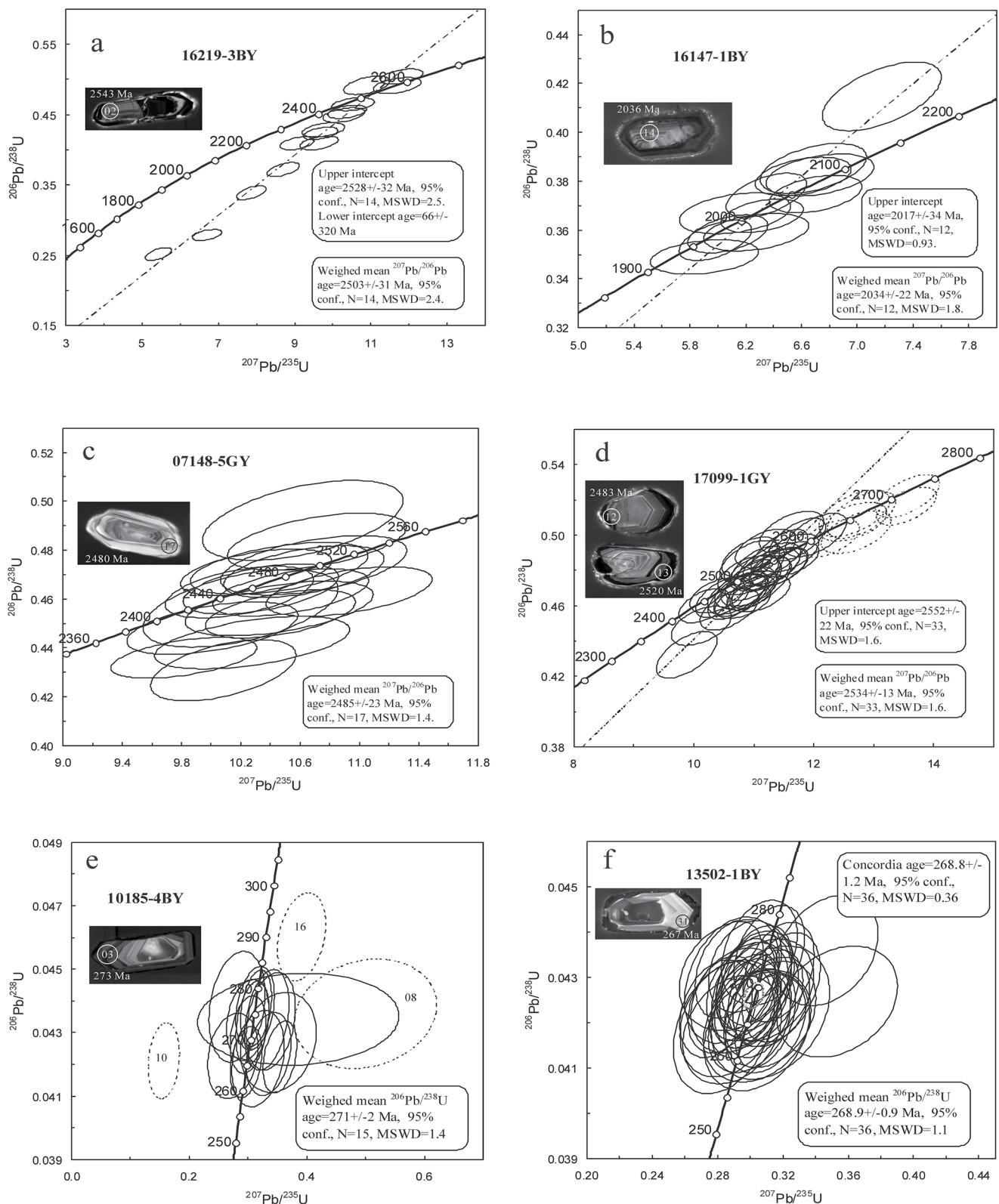### 4.2.1. Basement Rocks in the NCA

Fifteen spots on zircon grains from the granitic gneiss sample 16219-3BY collected from the basement rocks southwest to the Bayan Obo deposit were analyzed and 14 spots yield an upper intercept age of 2,528 ± 32 Ma and a lower intercept age of 66 ± 320 Ma (95% confidence, $N = 14$, MSWD = 2.5), and a weighted mean $^{207}Pb/^{206}Pb$ age of 2,503 ± 31 Ma (95% confidence, $N = 14$, MSWD = 2.4, Figure 4a). Eighteen spots on zircons from the granitic gneiss sample 16147-1BY collected from the core of the Kuangou anticline north to the Bayan Obo deposit were analyzed. Excluding 4 inherited zircons (spots 05, 06, 13, 17) and two discordant analyses (01, 03), the remaining spots yield an upper intercept age of 2,017 ± 34 Ma (95% confidence, $N = 12$, MSWD = 0.93) and a weighted mean $^{207}Pb/^{206}Pb$ age of 2,034 ± 22 Ma (95% confidence, $N = 12$, MSWD = 1.8, Figure 4b). Eighteen spots on zircons from the granitic gneiss sample 07148-5GY collected near Erjutu 40 km north to Guyang were analyzed, and except for one anomalous analysis (spot 04), the remaining analyses yield a weighted mean $^{207}Pb/^{206}Pb$ age of 2,485 ± 23 Ma (95% confidence, $N = 17$, MSWD = 1.4, Figure 4c). Forty analyses were performed on zircon grains from the granitic gneiss sample 17099-1GY located 16 km north to Guyang. Except for 7 inherited zircons (spots 21, 26, 27, 29, 33, 37, 40), the remaining analyses yield an upper intercept age of 2,552 ± 22 Ma (95% confidence, $N = 33$, MSWD = 1.6) and a weighted mean $^{207}Pb/^{206}Pb$ age of 2,534 ± 13 Ma (95% confidence, $N = 33$, MSWD = 1.6, Figure 4d). Zircons from the above samples are characterized by high Th/U ratios (0.15−1.82) and well-developed oscillatory zoning (Figures 4a–4d; Figures S2−S5 in Supporting Information S1), indicating a magmatic origin. Therefore, the above upper intercept or weighted mean $^{207}Pb/^{206}Pb$ ages reflect the crystalization ages of the granitic gneisses. These ages of ca. 2,500 Ma are similar to the previously reported ages of the TTG gneisses from the basement complex in the Yinshan Block (Jian et al., 2012; X. H. Zhang et al., 2014) and the crystallization age of ca. 2,017 Ma (sample 16147-1BY) indicates the existence of Paleoproterozoic granitic magmatism in the Yinshan Block.

### 4.2.2. Late Paleozoic Plutons in the NCA

Eighteen spots on zircons from the granite sample 10185-4BY collected from the Permian pluton near the eastern margin of the Bayan Obo deposit were analyzed and 15 corcondant analyses yield a weighted mean $^{206}Pb/^{238}U$ age of 271 ± 2 Ma (95% confidence, $N = 33$, MSWD = 1.6, Figure 4e). Fourteen analyses on zircons from the gneissic granite sample 13502-1BY collected from the Permian granite pluton 4 km south to the Bayan Obo deposit were analyzed and the concordant analyses yield a concordia age of 268.8 ± 1.2 Ma (95% confidence, $N = 36$, MSWD = 0.36) and weighted mean $^{206}Pb/^{238}U$ age of 268.9 ± 0.9 Ma (95% confidence, $N = 36$, MSWD = 1.1, Figure 4f). Zircons from the above two samples exhibited euhedral prismatic morphology, well-developed oscillatory zoning (Figures 4e and 4f; Figures S6 and S7 in Supporting Information S1) and high Th/U ratios (0.32–0.84), indicating that they are magmatic in origin. The ages of the above two samples are similar to those of the late Paleozoic dioritic-granitic plutons in the Bayan Obo and Guyang areas (Fan et al., 2009; X. H. Zhang et al., 2012; S. H. Zhang & Zhao, 2017).

4.2.3. Basement Rocks in the Retroarc Foreland

Thirty-five spots on 24 zircon grains from sample 17107-1GY collected from the Neoarchean to Paleoproterozoic metamorphic basement rocks 15 km south to Guyang were analyzed and are characterized by a wide range of $^{207}Pb/^{206}Pb$ ages from 2,440 to 1,868 Ma (Figure 5a). On probability density plot, they exhibit 3 main peaks of 2,394, 2,280, and 2,081 Ma and a minor peak of 1,880 Ma (Figure 5b). Thirty-five spots on 26 zircon grains from sample 17108-1BT collected from the Neoarchean to Paleoproterozoic metamorphic basement rocks 15 km east to Baotou were analyzed and the analytical spots exhibit a wide range of $^{207}Pb/^{206}Pb$ ages from 2,800 to 1,852 Ma (Figure 5c). On probability density plot, they exhibit two main peaks of 2,435 and 1,920 Ma and two minor peaks of 2,809 and 2,093 Ma (Figure 5d). Some zircon grains from these two samples show core-rim structure

Figure 4. U-Pb concordia diagrams for zircons from the Neoarchean to Paleoproterozoic metamorphic basement rocks and Permian plutons in the NCA. Data-point error crosses are 2σ.
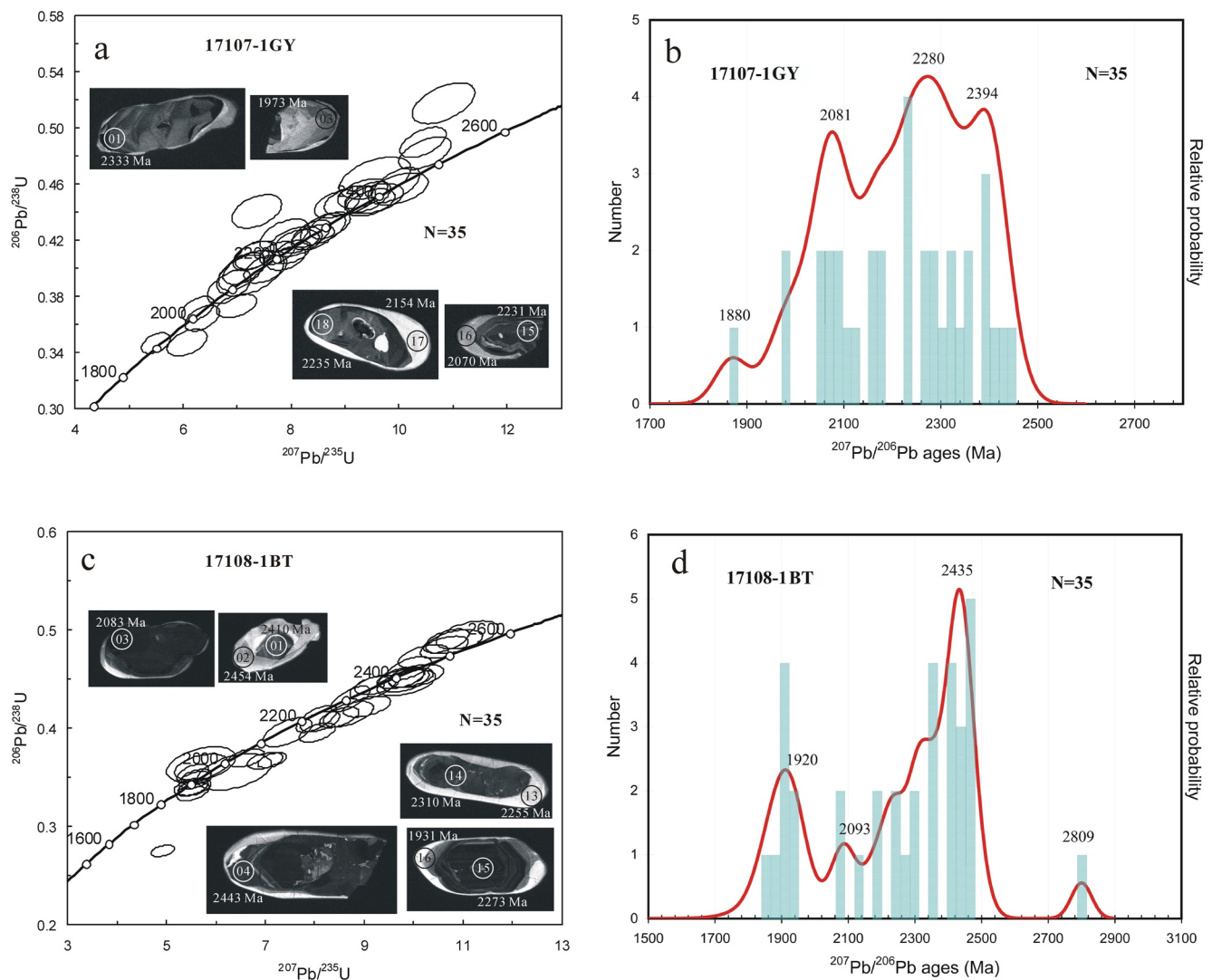
Figure 5. U-Pb Concordia (a and c) and probability density plots (b and d) diagrams for zircons from the Paleoproterozoic metamorphic basement rocks south to the western part of NCA. Data-point error crosses are 2σ.

(Figure 5; Figures S8 and S9 in Supporting Information S1), indicating a complex origin for these zircons. Most zircons of around 1,880−1,980 Ma are characterized by low concentrations of Th (0.065−141 ppm, mostly <50 ppm), U (7.7−412 ppm, mostly <100 ppm) and low or variable Th/U ratios (0.00−7.16), and are interpreted as metamorphic in origin. Most of other zircons are characterized by high Th/U ratios (0.24−1.03) and are interpreted as magmatic in origin. Some light rims (spots 08, 10, 17, 28, 29 and 32 from sample 17107-1GY; spots 02, 08, 13, 16, 20, 24, 26, 27, and 34 from sample 17108-1BT) with low contents of Th (24.4−168, mostly <100 ppm), U (7.4−375, mostly <130 ppm) and variable Th/U ratios (0.33−9.27) are interpreted as metamorphic in origin (Figure 5; Figures S8 and S9 in Supporting Information S1). Therefore, these two samples were most likely formed through metamorphism of Paleoproterozoic sedimentary rocks at 1,880−1,920 Ma during the collision between the Yinshan and Ordos blocks (Zhao et al., 2005).
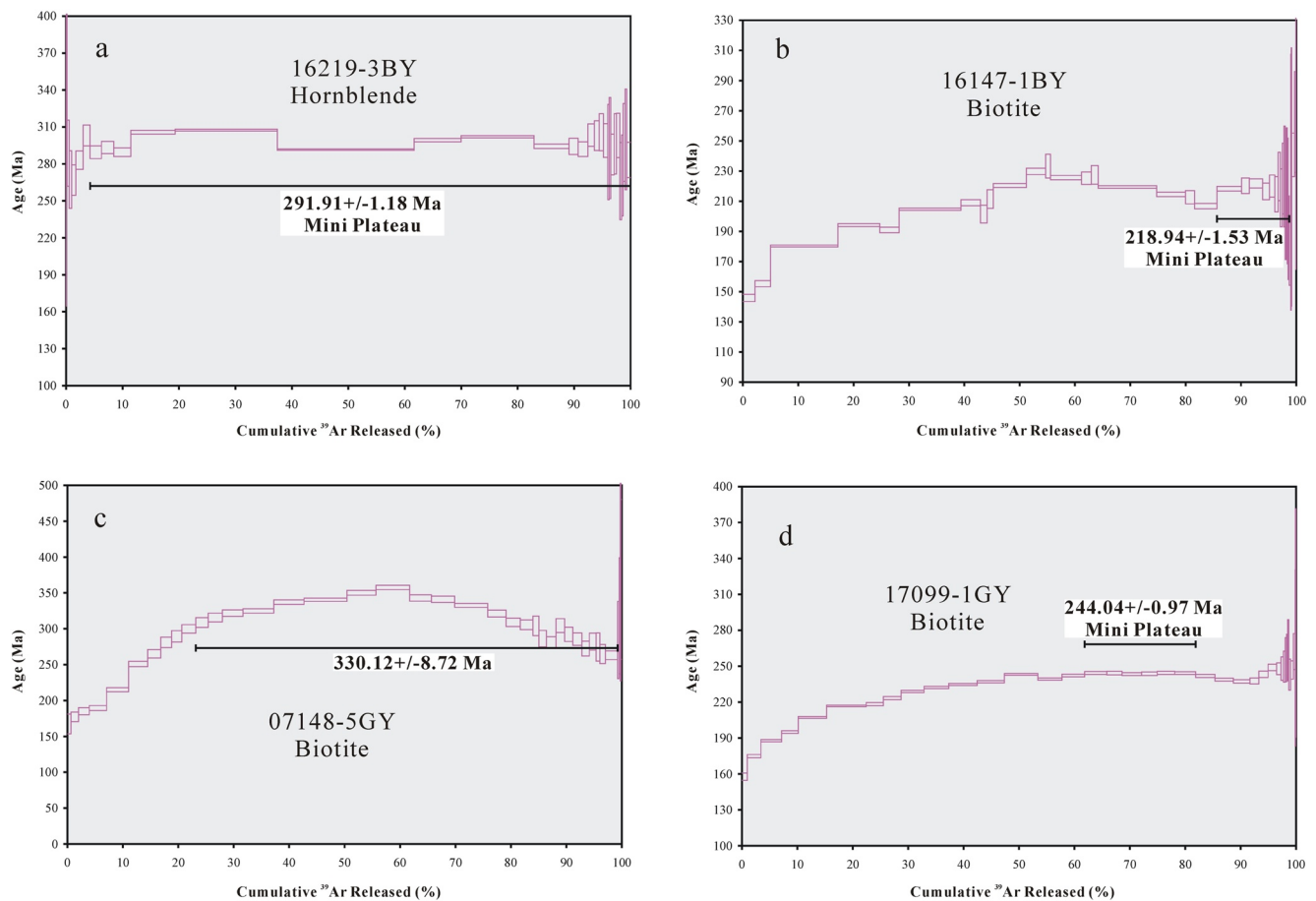
4.3. $^{40}Ar/^{39}Ar$ Ages

The $^{40}Ar/^{39}Ar$ incremental heating analytical results of 17 hornblende, muscovite and biotite samples from 13 samples were listed in Table S5−S21 and summarized in Table 3. The $^{40}Ar/^{39}Ar$ age spectra were plotted in Figures 6−9 and the inverse isochron plots were shown in Figure S10 in Supporting Information S1.

Table 3
Summary of the $^{40}Ar/^{39}Ar$ Incremental Heating Analytical Results of Hornblende, Muscovite, and Biotite From the Samples for Thermochronometric Investigations

Sample no.	Mineral	Age spectrum					n	N	Total fusion			Inverse isochron analyses		
		Age ± 2σ (Ma)	^{39}Ar (%)	K/Ca ± 2σ	MSWD				Age ± 2σ (Ma)	K/Ca ± 2σ	Age ± 2σ (Ma)	$^{40}Ar/^{36}Ar$ intercept	MSWD
16219-3BY	Hornblende	**291.91 ± 1.18**	48.55	0.309 ± 0.261	1.72	21	32	298.13 ± 1.16	0.473 ± 0.047	294.42 ± 2.11	183.36 ± 58.68	1.31
16147-1BY	Biotite	**218.94 ± 1.53**	13.08	0.31 ± 0.93	1.10	14	39	206.39 ± 0.83	5.35 ± 5.40	211.74 ± 10.18	347.54 ± 64.01	0.90
07148-5GY	Biotite	330.12 ± 8.72	88.28	0.11 ± 2.62	88.28	25	39	303.97 ± 1.39	2.05 ± 1.31	**255.30 ± 18.96**	1,534.98 ± 287.50	23.68
17099-1GY	Biotite	**244.04 ± 0.97**	20.04	21.6 ± 27.1	0.43	6	39	230.20 ± 0.81	21.6 ± 48.4	243.85 ± 11.79	302.56 ± 210.35	0.54
10185-4BY	Hornblende	**268.95 ± 1.22**	76.28	0.127 ± 0.035	1.21	20	32	269.63 ± 1.53	0.120 ± 0.007	267.35 ± 1.94	412.39 ± 93.38	1.07
10185-4BY	Biotite	297.53 ± 1.98	58.92	1.21 ± 0.82	1.46	15	39	246.41 ± 0.91	1.26 ± 0.29	301.20 ± 9.61	269.40 ± 133.41	9.73
13502-1BY	Biotite	253.24 ± 1.13	68.69	9.2 ± 19.0	5.74	13	39	**268.14 ± 1.68**	7.1 ± 7.1	251.24 ± 4.64	422.37 ± 189.78	5.84
07173-1	Hornblende	**279.16 ± 1.45**	100.00	1.704 ± 3.623	1.05	31	31	278.97 ± 1.73	0.102 ± 0.005	279.32 ± 1.96	446.61 ± 87.38	1.18
07173-1	Biotite	**256.94 ± 0.96**	78.85	29 ± 56	1.75	17	39	255.91 ± 0.97	359 ± 21638	257.39 ± 1.04	236.60 ± 52.82	1.45
08603-1	Hornblende	**280.94 ± 1.08**	100.00	0.097 ± 0.058	0.59	31	31	281.95 ± 1.40	0.086 ± 0.003	281.22 ± 1.34	261.93 ± 82.08	0.64
08603-1	Biotite	**273.39 ± 0.99**	45.70	47.4 ± 95.7	0.93	18	39	272.55 ± 0.97	14.8 ± 18.6	273.81 ± 1.14	141.35 ± 35.17	1.07
09219-1	Muscovite	**264.2 ± 1.8**	82.9	–	0.28	8	12	–	–	261.1 ± 6.7	549 ± 710	11.9
09243-2	Muscovite	**319.6 ± 3.4**	36.1	–	2.1	3	12	–	–	–	–	–
17105-1GY	Muscovite	**389.81 ± 1.74**	21.46	11.1 ± 10.1	0.58	3	39	402.14 ± 1.61	7.5 ± 15.0	386.99 ± 5.52	329.20 ± 56.94	0.01
17107-1GY	Biotite	**1,799 ± 5**	42.76	3.1 ± 9.2	1.90	16	39	1,793 ± 4	22.4 ± 55.0	1,806 ± 7	1,757.00 ± 835.69	1.45
17108-1BT	Hornblende	**1,880 ± 5**	99.97	0.117 ± 0.026	1.89	28	29	1,883 ± 5	0.152 ± 0.005	1,877 ± 6	3,355.54 ± 1,179.67	3.15
17108-1BT	Biotite	**1,897 ± 5**	48.17	2.9 ± 17.0	0.84	9	39	1,858 ± 5	7.6 ± 5.2	1,889 ± 11	2,004.82 ± 705.91	4.04

Note. The bold values in Table 3 are $^{40}Ar/^{39}Ar$ cooling ages being used in this study.
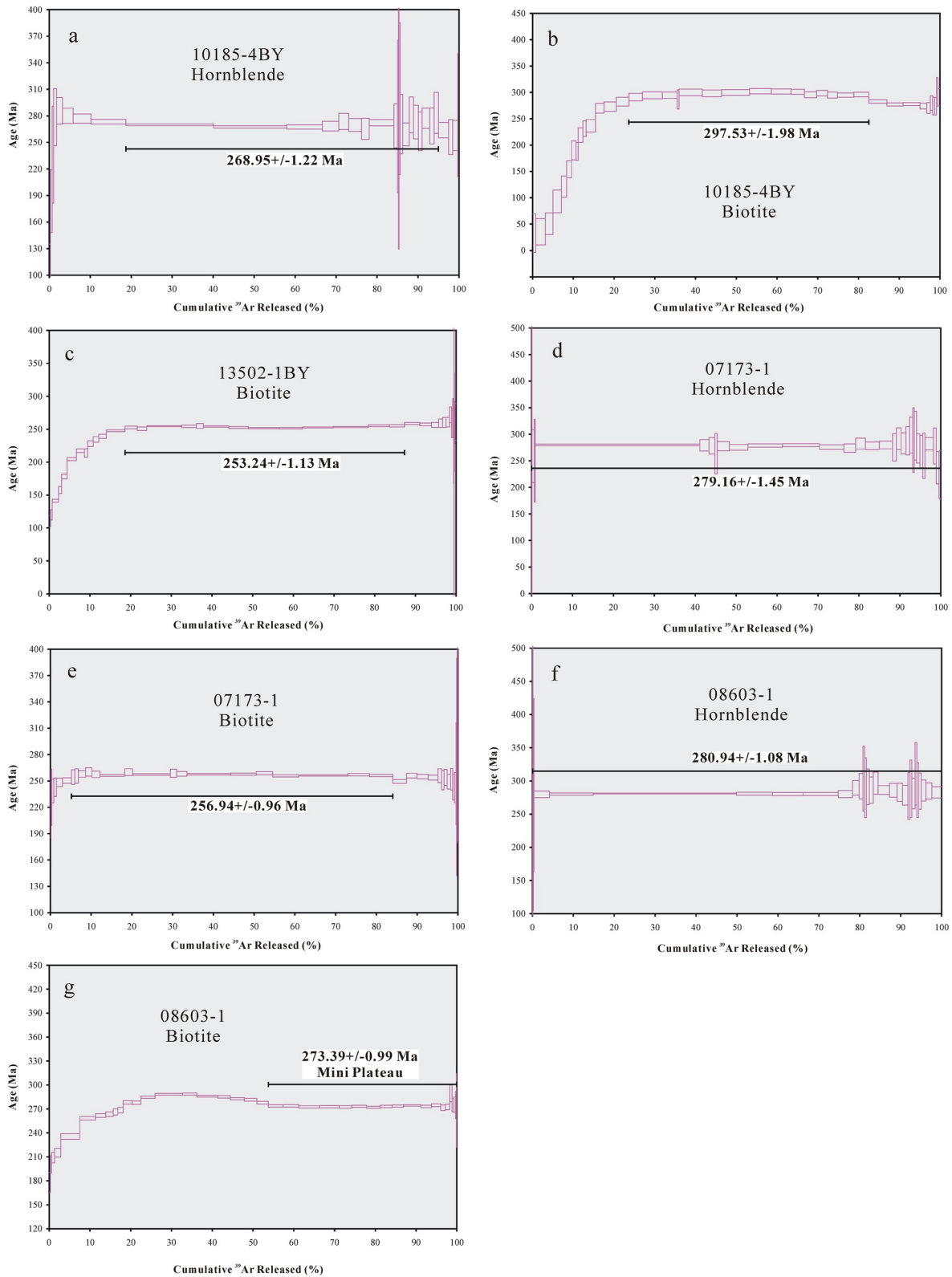
Figure 6. High-resolution incremental heating $^{40}Ar/^{39}Ar$ age spectra for hornblende and biotite samples from the basement complexes in the NCA. The $^{40}Ar/^{39}Ar$ ages are plateau ages and weighted mean ages with errors reported at the 2σ (95% confidence level).
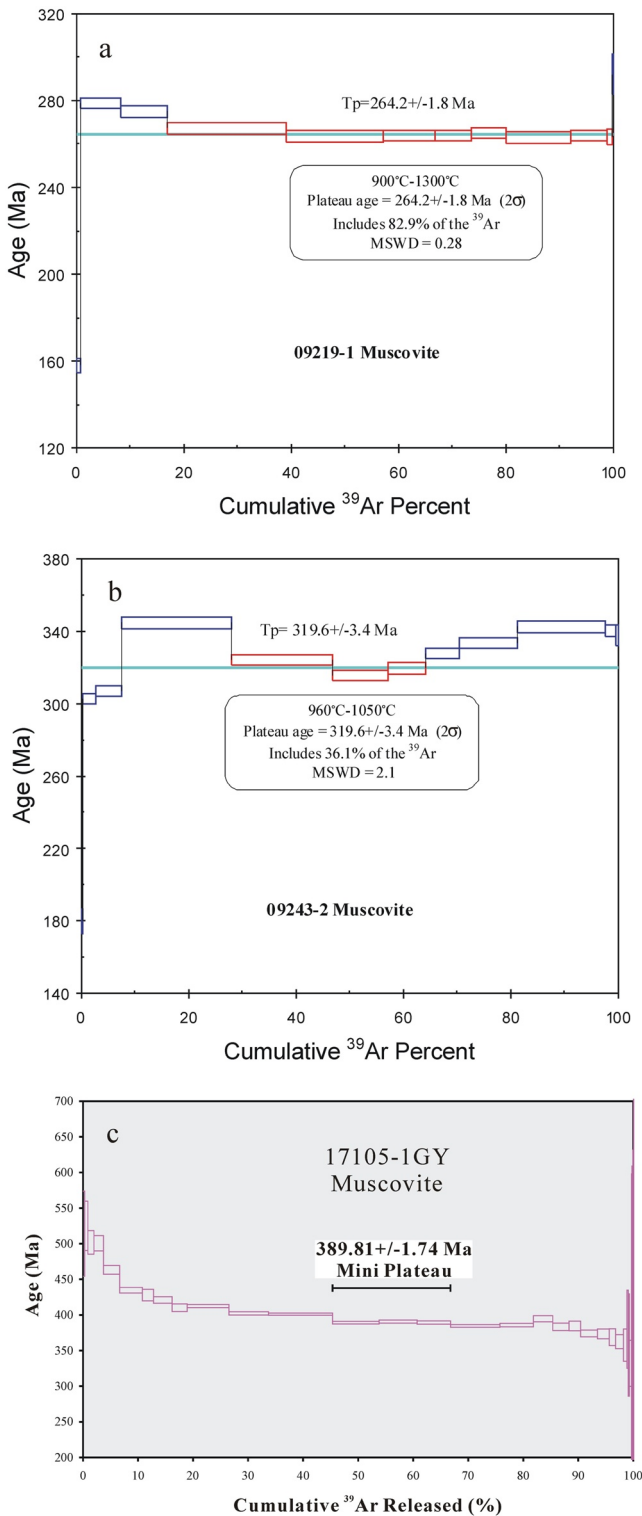
4.3.1. Basement Complexes in the NCA

Hornblende from sample 16219-3BY has a mini-plateau age of 291.91 ± 1.18 Ma ($\pm 2\sigma$, MSWD $= 1.72$, 48.55% ^{39}Ar gas released, Figure 6a). Biotite from the sample 16147-1BY is characterized by a slightly disturbed age spectrum and has a mini-plateau age of 218.94 ± 1.53 Ma (MSWD $= 1.10$, 13.08% ^{39}Ar released, Figure 6b). Biotite from the sample 07148-5GY exhibits a highly disturbed age spectrum due to chloritization, and has an imprecise plateau age of 330.12 ± 8.72 Ma (MSWD $= 88.28$, 76.07% ^{39}Ar released, Figure 6c). The total fusion and inverse isochron ages of this sample are 303.97 ± 1.39 and 255.30 ± 18.96 Ma (MSWD $= 23.68$), respectively (Table 3). We assigned the inverse isochron age of 255.30 ± 18.96 Ma as age for the biotite of the sample 07148-5GY (Figure S10c in Supporting Information S1). Biotite from the sample 17099-1GY has a mini-plateau age of 244.04 ± 0.97 Ma (MSWD $= 0.43$, 20.04% ^{39}Ar released, Figure 6d). Except for biotite from sample 07148-5GY exhibiting a highly disturbed age spectrum due to chloritization, the plateau ages of other samples are similar to their inverse isochron ages (Figures S10a, S10b, and S10d in Supporting Information S1), indicating reliability of the $^{40}Ar/^{39}Ar$ ages.

4.3.2. Late Paleozoic Plutons in the NCA

Hornblende from the sample 10185-4BY has a plateau age of 268.95 ± 1.22 Ma (MSWD $= 1.21$, 76.28% ^{39}Ar released, Figure 7a). Biotite from this sample 10185-4BY has a plateau age of 297.53 ± 1.98 Ma (MSWD $= 1.46$, 58.92% ^{39}Ar released, Figure 7b) and total fusion age of 268.14 ± 1.68 Ma (Table 2). Since biotite plateau age of 297.53 ± 1.98 Ma is older than zircon U-Pb age of 271 ± 2 Ma of sample 10185-4BY (Figure 4e) due to existence of excess argon or alteration, we assigned the total fusion age of 268.14 ± 1.68 Ma as approximate age for the biotite of the sample 10185-4BY. Biotite from the sample 13502-1BY has a plateau age of 253.24 ± 1.13 Ma (MSWD $= 5.74$, 68.69% ^{39}Ar released, Figure 7c). Hornblende and biotite from the sample 07173-1 have plateau

Figure 7. High-resolution incremental heating ^{40}Ar/^{39}Ar age spectra for hornblende and biotite samples from the late Paleozoic plutons in the NCA. The ^{40}Ar/^{39}Ar ages are plateau ages and weighted mean ages with errors reported at the 2σ (95% confidence level).

ages of 279.16 ± 1.45 Ma (MSWD = 1.05, 100% ^{39}Ar released, Figures 7d) and 256.94 ± 0.96 Ma (MSWD = 1.75, 78.58% ^{39}Ar released, Figure 7e), respectively. Hornblende and biotite from the sample 08603-1 have plateau ages of 280.94 ± 1.08 Ma (MSWD = 0.59, 100% ^{39}Ar released, Figures 7f) and 273.39 ± 0.99 Ma (MSWD = 0.93, 45.70% ^{39}Ar released, Figure 7g), respectively. Since biotite from sample 08603-1 exhibiting slight hump-shape of age spectrum may be indicative of excess argon in the early released gas (McLaren et al., 2009; Schwarz & Lippolt, 2014), the high-temperature steps were selected to calculate plateau age to avoid influence of excess argon. Except for biotite from sample 10185-4BY, the plateau ages of other samples are similar to their inverse isochron ages (Figures S10e, S10g−S10k in Supporting Information S1), indicating that the ^{40}Ar/^{39}Ar ages are reliable.

4.3.3. Mesoproterozoic and Silurian Schists in the Northern Margin of the NCA

Muscovite from sample 09219-1 has a plateau age of 264.2 ± 1.8 Ma (MSWD = 0.28, 82.9% ^{39}Ar released, Figure 8a). The isochron and inverse isochron ages of this sample are 265.5 ± 3.4 Ma (MSWD = 0.89) and 261.1 ± 6.7 Ma (MSWD = 11.9), respectively (Table 3), and are similar to its plateau age of 264.2 ± 1.8 Ma. Muscovite from sample 09243-2 is characterized by slightly disturbed age spectrum with a plateau age of 319.6 ± 3.4 Ma (MSWD = 2.1, 36.1% ^{39}Ar released, Figure 8b).

4.3.4. Mesoproterozoic Slate in the Southern Margin of the NCA

Muscovite from sample 17105-1GY is characterized by slightly disturbed age spectrum and has a mini-plateau age of 389.91 ± 1.74 Ma (MSWD = 0.58, 21.46% ^{39}Ar released, Figure 8c). The above mini-plateau age is similar to the inverse isochron age of 386.99 ± 5.52 Ma (MSWD = 0.01, Figure S10l in Supporting Information S1) of this sample.
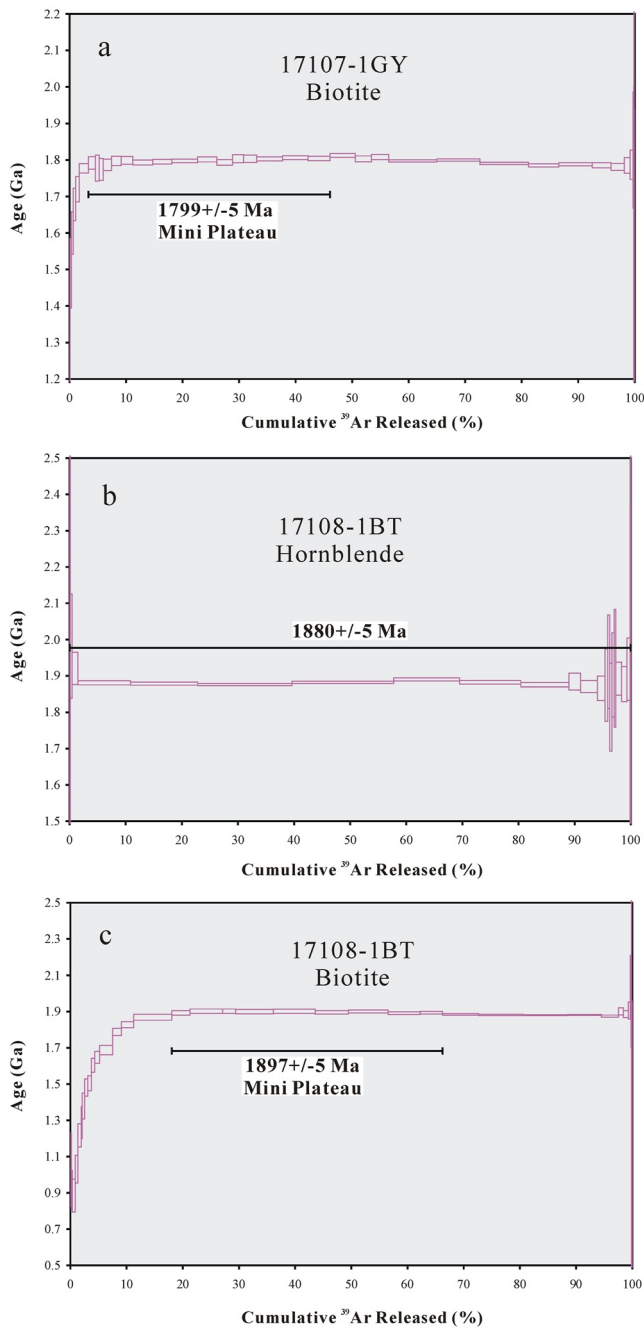
4.3.5. Basement Complexes in the Retroarc Foreland

Biotite from sample 17107-1GY has a mini-plateau age of 1,799 ± 5 Ma (MSWD = 1.90, 42.76% ^{39}Ar released, Figure 9a). Hornblende and biotite from the sample 17108-1BT have plateau ages of 1,880 ± 5 Ma (MSWD = 1.89, 99.97% ^{39}Ar released, Figures 9b) and 1,897 ± 5 Ma (MSWD = 0.84, 48.17% ^{39}Ar released, Figure 9c), respectively. The plateau ages of these samples are similar to their inverse isochron ages (Figures S10m−S10o in Supporting Information S1).

5. Discussion

5.1. Emplacement Depth Variations in the Western Part of the NCA

As shown in Table 2 and Table S3, the newly obtained and recalculated crystallization pressure data obtained by the Al-in-hornblende barometer show that emplacement depths of the Carboniferous-Permian arc plutons in the western part of the late Paleozoic NCA decrease from south to north with the maximum emplacement depths of ca. 15 km in the southern and central parts of the NCA and the minimum emplacement depths of ca. 6 km in the northern part of the NCA (Figure 2).

The above emplacement depths are consistent with geological evidence in these areas (e.g., Jia et al., 2003; Z. H. Liu et al., 2003; S. H. Zhang et al., 2016). The Carboniferous-Permian arc plutons intruded mainly into the Meso-Neoproterozoic Bayan Obo group (Figure 2) and exhibit massive

Figure 8. High-resolution incremental heating ^{40}Ar/^{39}Ar age spectra for hornblende and biotite samples from the Mesoproterozoic and Silurian schists in the NCA. The ^{40}Ar/^{39}Ar ages are plateau ages and weighted mean ages with errors reported at the 2σ (95% confidence level).

Figure 9. Incremental heating $^{40}Ar/^{39}Ar$ age spectra for hornblende and biotite samples from the basement complexes in the retroarc foreland. The $^{40}Ar/^{39}Ar$ ages are plateau ages and weighted mean ages with errors reported at the 2σ (95% confidence level).

structure without ductile deformation. The Noearchean-Paleoproterozoic metamorphosed basement rocks are occasionally exposed around Bayan Obo and the Permian volcanic rocks with zircon U-Pb ages of 278−261 Ma are well preserved (S. H. Zhang et al., 2016). This geological evidence indicates emplacement of the Carboniferous-Permian plutons around Bayan Obo in the northern part of the NCA in shallow crustal levels, most likely less than 6 km. In constrast, the Carboniferous-Permian arc plutons in the southern and central parts of the NCA around Guyang emplaced mainly into the Noearchean-Paleoproterozoic metamorphosed basement rocks (Figure 2) and some of them exhibit ductile deformation with foliations parallel to their host rocks (Wu et al., 2014). The Noearchean-Paleoproterozoic metamorphosed basement rocks are extensively exposed and no Paleozoic volcanic or sedimentary rocks exist around Guyang (Figure 2). The above geological evidence is consistent with emplacement of the Carboniferous-Permian arc plutons in the southern and central parts of the NCA around Guyang in deeper crustal levels at 9−15 km (Figure 2 and Table S3).

5.2. Late Paleozoic Thermal State of the Mid- to Upper-Crust

The Permian plutons are mostly characterized by high cooling rates of 131.1–321.4°C/Ma from 800 ± 50°C (zircon U-Pb closure temperature) to 530 ± 50°C (hornblende Ar/Ar closure temperature) and of 10.4–283.9°C/Ma from 530 ± 50 to 300 ± 50°C (biotite Ar/Ar closure temperature) (Figure 10). These high cooling rates are consistent with the emplacement of the plutons in mid-to upper-crustal levels at depths from ca. 15 to ca. 6 km (Table 2 and Table S3), and are distinctly different from those of the late Carboniferous-Permian granitic batholith that was emplaced at the mid-crustal levels with a slow cooling rate of 4.9–5.0°C/Ma in the middle part of the NCA (S. H. Zhang et al., 2019). The plutons in the northern part of the NCA with shallow emplacement depths of ca. 6.0 km (East Bayan Obo granitic pluton, Figure 2) have relatively higher cooling rates (283.9°C/Ma, Figure 10a) from 530 ± 50°C to 300 ± 50°C than those of the plutons in central and southern parts of the NCA (Rentaihe and Yinhao plutons, 10.4–30.0°C/Ma, Figures 10c and 10d) with deep emplacement depths of 9.0–14.8 km (Figure 2).

Although the ca. 2,550 and ca. 2,017 Ma basement complexes in the NCA (samples 16219-3BY, 16147-1BY, 07148-5GY, and 17099-1GY) are not in direct contact with the late Paleozoic plutons and are about 500 m to several 10 km away from these plutons, they have hornblende and biotite $^{40}Ar/^{39}Ar$ ages from 291.91 ± 1.18 to 218.94 ± 1.53 Ma. Muscovite from the Mesoproterozoic slate of the Agulugou Formation (sample 17105-1GY) near the southern margin of the NCA has an $^{40}Ar/^{39}Ar$ age of 389.91 ± 1.74 Ma. Muscovite separates from the Mesoproterozoic and Silurian schists (samples 09219-1, 09243-2) near the northern margin of the NCA have $^{40}Ar/^{39}Ar$ ages of 264.2 ± 1.8 and 319.6 ± 3.4 Ma, respectively. Since all these rocks were located in the mid-to upper-crustal levels during the late Paleozoic, these late Paleozoic to Triassic $^{40}Ar/^{39}Ar$ ages indicate that the mid-to upper-crust of the NCA were strongly heated and remained hot during the Permian-Triassic period with crustal temperatures of >530 ± 50°C (hornblende Ar/Ar closure temperature) or > 300 ± 50°C (biotite Ar/Ar closure temperature). This warm thermal state of the mid-to upper-crust in the western part of the NCA is consistent with our previous results on the middle part of the NCA, in which the mid-to upper-crust remained warm (>530 ± 50°C) during the arc construction at 320–260 Ma (S. H. Zhang et al., 2019). The $^{40}Ar/^{39}Ar$ ages of biotite and muscovite exhibit a younger trend from south to north in the NCA, which is supported by the muscovite $^{40}Ar/^{39}Ar$ ages of two
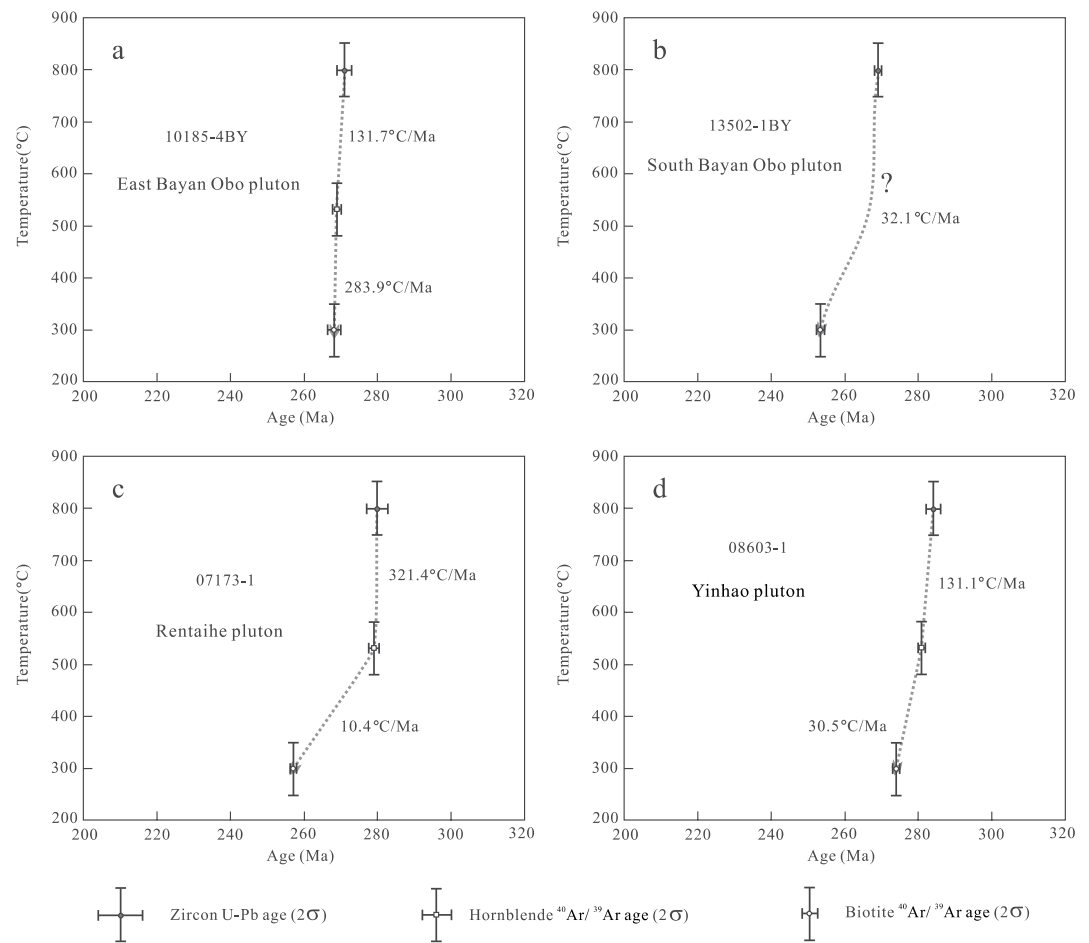
Figure 10. Diagrams showing the reconstructed cooling paths and cooling rates of the Permian plutons in the western part of the NCA. Closure temperatures (zircon U-Pb: 800 ± 50°C; hornblende Ar/Ar: 530 ± 50°C; muscovite Ar/Ar: 350 ± 50°C; biotite Ar/Ar: 300 ± 50°C) are compiled from Chew and Spikings (2015), Gehrels et al. (2003), Hodges (2014), McDougall and Harrison (1999), Nadin et al. (2016), Noury et al. (2021), and Saleeby et al. (2007).

samples (17105-1GY, 09219-1) of the metamorphosed Mesoproterozoic sedimentary rocks in the southern and northern margins of the NCA.

In contrast, the Paleoproterozoic basement complexes of the retroarc foreland have hornblende and biotite ^{40}Ar/^{39}Ar ages of 1,897 ± 5 to 1,799 ± 5 Ma, indicating a cold (<300 ± 50°C) upper-crust that was not thermally modified during the late Paleozoic. Although Triassic intrusions are common in this area, they had no thermal disturbance on the thermal state of the upper-crust.

5.3. An Unusually Warm Upper-Crust Around Bayan Obo During the Late Paleozoic

Continental arcs are usually characterized by relatively low average geothermal gradients (ca. 15°C/km) due to the thick crust usually of >60 km (e.g., Cao et al., 2019; Saltus & Lachenbruch, 1991). However, since the mid-to upper-crust of a continental arc represents one of the most important sites of intensive intrusion of dioritic-granitic batholiths and plutons, it may have high geothermal gradients of 30–50°C/km as a result of the heat transfer due to magma migration (Cao et al., 2019; Rothstein & Manning, 2003; S. H. Zhang et al., 2019). Our previous thermochronometric results for basement rocks and arc plutons exhumed from the mid-to upper-crust (18.7–13.8 km) across the middle part of the NCA indicate that during the late Paleozoic, the mid-to upper-crust of the arc was warm with average paleogeothermal gradients of 37.0–44.5°C/km and the mid- to upper-crust beneath the retro-arc foreland to the south of the arc was cold with relatively low paleogeothermal gradients of <21.5°C/km (S. H. Zhang et al., 2019).

Our new zircon U-Pb and hornblende, muscovite and biotite ^{40}Ar/^{39}Ar ages of mid-to upper-crustal rocks (ca. 15 km to ca. 6 km, Figure 2, Table 2 and Table S3, recalculated from Wu et al., 2014; S. H. Zhang & Zhao, 2017) show that the mid-to upper-crust of the western part of the NCA has undergone strong thermal modifications during the late Paleozoic and resulted in complete resetting of hornblende, muscovite and biotite Ar/Ar isotopic systems. However, the upper-crust of the retroarc foreland south to the NCA has not been affected and is characterized by old hornblende and biotite ^{40}Ar/^{39}Ar ages of 1.90−1.80 Ga. Using the largest crustal depth of 14.8 km (sample 10224-1 from the Yinhao pluton northeast to Guyang, Figure 2, Table S3) and Ar/Ar closure temperature of biotite (300 ± 50°C), we obtain a minimal average geothermal gradient of 20.4 ± 3.4°C/km for the mid-to upper-crust of the western part of the NCA around Guyang. Maximal and minimal average geothermal gradients of 88.3 ± 8.3 and 50.0 ± 8.3°C/km can be obtained by using a crustal depth of ca. 6 km and Ar/Ar closure temperatures of hornblende (530 ± 50°C) and biotite (300 ± 50°C), respectively. The above upper-crust geothermal gradients of 50.0 ± 8.3 to 88.3 ± 8.3°C/km estimated by geothermobarometric data in the western part of the NCA around Bayan Obo during the late Paleozoic are significantly higher than those of other continental arcs (Cao et al., 2019; Rothstein & Manning, 2003 and references therein), indicative of the existence of an unusually warm upper-crust around Bayan Obo. However, due to limited geothermobarometric data obtained in this study, possible future studies are required to collect evidence supporting whether these unusually warm upper-crusts exist in other areas in the western part of the NCA.

The northward younging trend of biotite and muscovite ^{40}Ar/^{39}Ar ages (Figure 2, Table 3) indicates that thermal modifications of the upper-crust of the northern margin (Bayan Obo) of the western NCA were much stronger than that of the southern margin (Guyang). Since the emplacement depths of Permian plutons in the north are ca. 6 km, shallower than those (ca. 15 km) in the south (Figure 2, Table 2, and Table S3, recalculated from Wu et al. (2014) and S. H. Zhang and Zhao (2017)), the depths of the thermochronometric samples in the northern margin are shallower than those of the southern margin during the late Paleozoic. Therefore, the average upper-crust geothermal gradients of the western part of the NCA increase from south to north with the minimal geothermal gradient of 20.4 ± 3.4°C/km near Guyang in the south and the maximal geothermal gradient of 88.3 ± 8.3°C/km around Bayan Obo in the north. Since magmatic advection is the predominant heat transport mechanism that influences temperatures in the middle and upper-crust in magmatic arcs as previously suggested (e.g., Barton & Hanson, 1989; De Yoreo et al., 1991; Rothstein & Manning, 2003), we propose that magmatic advection during arc construction is the main mechanism for hot/warm mid- to upper-crust and high geothermal gradient in the NCA during the late Paleozoic. Moreover, since the Permian granitoids near Bayan Obo deposit are rich in heat-producing elements (U = 1.30−5.78 ppm, Th = 17.7−33.0 ppm, K_2O = 4.48−5.15 wt.%, Ling et al., 2014), prolonged radiogenic decay of heat-producing elements (particularly U, Th and K) in these granitoids (McLaren, Neumann, et al., 1999; McLaren, Sandiford, & Hand, 1999, 2003, 2005; McLaren & Powell, 2014; Sandiford et al., 2002; Wilson & Åkerblom, 1982) is likely another mechanism for high or extremely high geothermal gradient around Bayan Obo. The presence of fluids or volatiles during arc construction may enhance heat transport by magmatic advection; especially increase the vertical heat transfer (e.g., Bachmann & Bergantz, 2006; De Yoreo et al., 1991; Deming, 1994).

5.4. Implications for Modification of the Bayan Obo Deposit

The Bayan Obo deposit is associated with 1.32−1.30 Ga carbonatite sills and dykes in the northern part of the NCA (Figure 2). It is now clear that the Bayan Obo deposit was primarily formed at 1.32−1.30 Ga (Fan et al., 2016; Q. Li et al., 2018; K. F. Yang et al., 2019; S. H. Zhang, Zhao, Liu, et al., 2017; Zhu et al., 2015), consistent with the zircon U-Pb and Sm-Nd whole rock/mineral isochron ages of ca. 1,300 Ma (Q. Li et al., 2018; S. H. Zhang, Zhao, Liu, et al., 2017; Zhu et al., 2015). However, there are discrepancies among ^{208}Pb/^{232}Th ages of monazite and bastnäsite from this deposit and these ages range from ca. 1,320 to ca. 260 Ma (e.g., X.-C. Li et al., 2021, 2022; Ling et al., 2013; Song et al., 2018; Wei et al., 2022; K. F. Yang et al., 2019; Y. H. Yang et al., 2019). This large spread in ages of REE-bearing minerals resulted in confusion and intense controversy in interpreting the timing, genesis and episodes of REE mineralization in the Bayan Obo deposit (Fan et al., 2016; Ling et al., 2013; Smith et al., 2015; X. Y. Yang et al., 2017).

One possibility for this large spread was the strong thermal perturbations after the formation of the deposit, which resulted in complete or partial resetting of the (U-)Th-Pb isotopic system to explain the young and wide range of monazite and bastnäsite ^{208}Pb/^{232}Th ages (X.-C. Li et al., 2021, 2022; Song et al., 2018; K. F. Yang et al., 2019; Y. H. Yang et al., 2019; S. H. Zhang, Zhao & Liu, 2017). Although a few studies suggest that the closure

temperatures of the Th-(U-)Pb isotopic system of monazite and bastnäsite could be higher than 700°C (Cherniak et al., 2004; Copeland et al., 1988; Parrish, 1990), other studies show that these minerals are sensitive to hydrothermal alteration at temperatures well below diffusional closure temperatures, and disturbed and meaningless Th-(U-)Pb ages may be obtained even under temperatures lower than 400°C (Gysi & Williams-Jones, 2015; X. Li et al., 2020; Seydoux-Guillaume et al., 2012; Song et al., 2018; Teufel & Heinrich, 1997; Townsend et al., 2000; Williams et al., 2011; W. Zhang et al., 2023). For example, monazite dating results on the ca. 64 Ma Ireteba pluton intruded by two 16 Ma Miocene plutons show that even in rocks that are undeformed, distant from younger intrusions, and apparently unaltered, monazite was partly recrystallized under low temperatures of <400°C and has the same age as the younger intrusions (Townsend et al., 2000).

Thermogravimetric analysis and high-temperature Raman spectroscopy demonstrate that the decomposition temperature of bastnäsit-(Ce) is 400°C (673 K) and bastnäsite undergoes a decarbonization transition at above 400°C (X. Li et al., 2020). The decomposition temperature of bastnäsite-(La) is ca. 310°C (ca. 583 K, Janka & Schleid, 2009). The presence of F^- can largely enhance the thermal stability and incompressibility of bastnäsite (X. Li et al., 2020).

Originally the Bayan Obo deposit was formed in the upper-crust and remained so during the late Paleozoic until the Mesozoic, when the deposit was exhumed together with the country rocks, that is, the Banyan Obo Group. In the mining district, most of the REE ores are not in contact with the Carboniferous-Permian and Triassic plutons (Figure 2). Therefore, the thermal perturbations cannot be explained by the emplacement of these plutons.

REE mineralization in the Bayan Obo deposit is featured with the disseminated REE ores with an average grade of 3–5 wt.% REE_2O_3, and the vein-type, banded or massive REE ores with a relatively high REE_2O_3 grade of 8–10 wt.% (e.g., Fan et al., 2016; X.-C. Li et al., 2021; Song et al., 2018; K. F. Yang et al., 2019). The disseminated ores occur widely throughout the carbonate sills ("H8" dolomite) or dykes (Figures 11a and 11g), indicating crystallization of REE-bearing minerals from carbonatitic magmatism. The other types of ores occur near the contact between the carbonate sills and host slate, which may be related to late hydrothermal alteration and recrystallization of the early REE-bearing minerals (Figures 11b–11d, 11f, and 11g). Existence of abundant fluorite in the veined or banded ores (e.g., Deng et al., 2017; Fan et al., 2016; S. Liu et al., 2018, 2022; Shimazaki et al., 2008; Wei et al., 2022; X. Y. Yang et al., 2017; P. S. Zhang & Tao, 1986) indicates presence of F in the hydrothermal fluids, which would have enhanced the thermal stability and recrystallization of bastnäsite (Figures 11b, 11c, and 11h).

Our identification of an unusually warm upper-crust in the NCA during the late Paleozoic provides important insights about the thermal modification of the REE ores of the Bayan Obo deposit. As shown by the late Paleozoic hornblende and biotite $^{40}Ar/^{39}Ar$ ages from the upper-crustal basement complexes and Permian plutons around Bayan Obo, the upper-crust was heated above the closure temperatures of hornblende (530 ± 50°C) and biotite (300 ± 50°C) and was characterized by a high paleogeothermal gradient of >50.0 ± 8.3°C/km with a maximal geothermal gradient of 88.3 ± 8.3°C/km around Bayan Obo during this period. These upper-crust temperatures from 530 ± 50°C to 300 ± 50°C are higher than the decomposition temperature of bastnäsites from 400 to 310°C (Janka & Schleid, 2009; X. Li et al., 2020), and resulted in strong thermal perturbations and recrystallization of the thermal sensitive REE-bearing minerals such as monazite and bastnäsite. This warm upper-crust and high paleogeothermal gradients may provide a steady force to drive the hydrothermal fluids in the surrounding sedimentary rocks of the Bayan Obo Group and resulted in complex textures of ore bodies and enrichment of REE-bearing minerals in the veined, banded or massive ores. Abundant fluorite associated with the REE-bearing minerals in the Byan Obo deposit (e.g., Deng et al., 2017; Fan et al., 2004; S. Liu et al., 2018, 2022; Shimazaki et al., 2008; X. Y. Yang et al., 2017; P. S. Zhang & Tao, 1986) provides solid evidence for presence of F^- that may largely enhanced the thermal stability and incompressibility of bastnäsite (X. Li et al., 2020).

The late thermal perturbations and resetting of early formed carbonatite-related REE deposits may be critical to REE enrichment and formation of high-grade REE ores in Bayan Obo and other REE deposits such as the Yangibana REE deposits in Western Australia. These thermal events explain their complex REE mineral ages (Slezak et al., 2020; Slezak & Spandler, 2019; Zi et al., 2017), especially for deposits in areas with high paleogeothermal gradients and unusually warm upper-crust. Moreover, interpretations of the isotopic results of thermally sensitive minerals such as monazite and bastnäsite from REE ore bodies should be treated with caution in such deposits, because the early isotopic systems may have been completely or partially reset by younger thermal events and have no geological meanings (X.-C. Li et al., 2021, 2022; Song et al., 2018; S. H. Zhang, Zhao, Liu, et al., 2017, S. H. Zhang, Zhao & Liu, 2017).
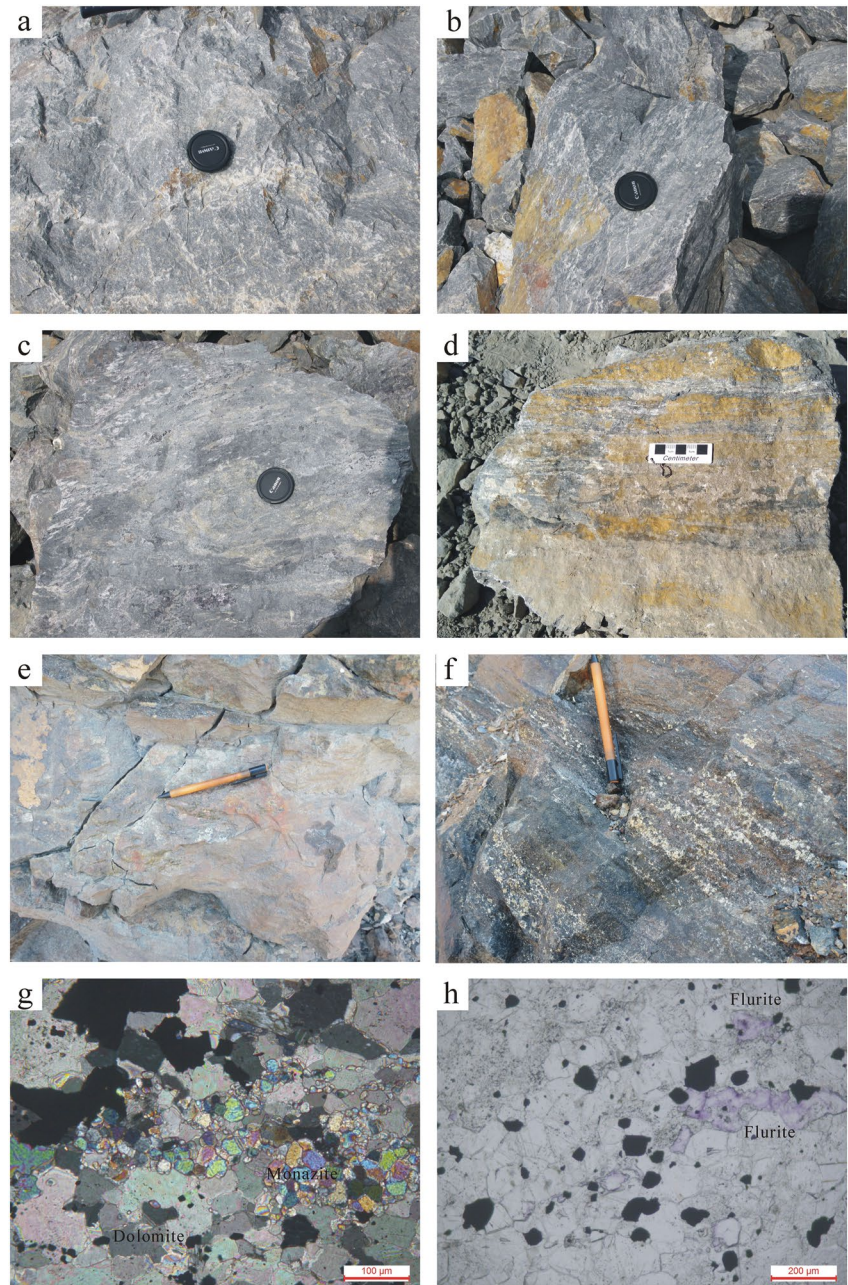
Figure 11. Representative outcrop and photomicrographs of major mineralization types from the giant Bayan Obo rare earth element (REE) deposit. (a) Carbonatite (dolomite) with disseminated mineralization in East ore body; (b and c) banded REE mineralization in East ore body and fluorite is common in banded ores; (d) banded REE ores in West ore body; (e) carbonatite (dolomite) with disseminated mineralization in an open pit east to the East ore body (N41°48.6′, E110°00.9′); (f) banded REE mineralization in an open pit east to the East ore body (N41°48.6′, E110°00.9′); (g) enrichment of REE minerals in banded ores from an open pit east to the East ore body (N41°48.5′, E110°00.5′); (h) fluorite in REE-rich carbonatite (dolomite) from an open pit east to the East ore body (N41°48.6′, E110°00.9′).

6. Conclusion

This study first reported the ^{40}Ar/^{39}Ar ages of the Archean to Permian rocks along a north−south corridor across the western part of NCA and its retroarc foreland. The results show that the mid- to upper-crust of the western part of the NCA has been strongly affected by thermal modifications during arc construction in the late Paleozoic and that of the retroarc foreland remains unaffected. The upper-crust under the Bayan Obo area, the western

part of the NCA, had high geothermal gradients of 50.0 ± 8.3 to $88.3 \pm 8.3°C/km$ and was thus unusually warm during the late Paleozoic, which resulted strong thermal perturbations and recrystallization of the thermal sensitive REE-bearing minerals such as monazite and bastnäsite in the Bayan Obo deposit, as well as enrichment and formation of high-grade REE ores and complete or partial resetting of the (U-)Th-Pb isotopic system of monazite and bastnäsite. Our identification of the unusually warm upper-crust provides important constraints on the genesis and thermal modifications of the Bayan Obo REE deposit and explains well the large variable monazite and bastnäsite $^{208}Pb/^{232}Th$ ages, as well as the upper-crustal thermal state of the NCA during the late Paleozoic.

Conflict of Interest

The authors declare no conflicts of interest relevant to this study.

Data Availability Statement

Supporting data for this study are provided in Texts S1 and S2 and Figures S1−S10 in Supporting Information S1 and Tables S1−S21, and are available in the Mendeley Data at https://doi.org/10.17632/s98hbvshjd.3.

References

Ague, J. J. (1997). Thermodynamic calculation of emplacement pressures for batholithic rocks, California: Implications for the aluminum-in-hornblende barometer. *Geology*, *25*(6), 563–566. https://doi.org/10.1130/0091-7613(1997)025<0563:tcoepf>2.3.co;2

Anderson, J. L., Barth, A. P., Wooden, J. L., & Mazdab, F. (2008). Thermometers and thermobarometers in granitic systems. *Reviews in Mineralogy and Geochemistry*, *69*(1), 121–142. https://doi.org/10.2138/rmg.2008.69.4

Anderson, J. L., & Smith, D. R. (1995). The effects of temperature and fO$_2$ on the Al-in-hornblende barometer. *American Mineralogist*, *80*(5–6), 549–559. https://doi.org/10.2138/am-1995-5-614

Bachmann, O., & Bergantz, G. W. (2006). Gas percolation in upper crustal silicic crystal mushes as a mechanism for upward heat advection and rejuvenation of near-solidus magma bodies. *Journal of Volcanology and Geothermal Research*, *149*(1–2), 85–102. https://doi.org/10.1016/j.jvolgeores.2005.06.002

Barton, M. D., & Hanson, R. B. (1989). Magmatism and the development of low-pressure metamorphic belts: Implications from the Western United States and thermal modeling. *Geological Society of America Bulletin*, *101*(8), 1051–1065. https://doi.org/10.1130/0016-7606(1989)101<1051:matdol>2.3.co;2

Beck, S. L., Zandt, G., Myers, S. C., Wallace, T. C., Silver, P. G., & Drake, L. (1996). Crustal-thickness variations in the central Andes. *Geology*, *24*(5), 407–410. https://doi.org/10.1130/0091-7613(1996)024<0407:ctvitc>2.3.co;2

Campbell, L. S., Compston, W., Sircombe, K. N., & Wilkinson, C. C. (2014). Zircon from the East Orebody of the Bayan Obo Fe–Nb–REE deposit, China, and SHRIMP ages for carbonatite-related magmatism and REE mineralization events. *Contributions to Mineralogy and Petrology*, *168*(2), 1041. https://doi.org/10.1007/s00410-014-1041-3

Cao, W., Lee, C.-T. A., Yang, J., & Zuza, A. V. (2019). Hydrothermal circulation cools continental crust under exhumation. *Earth and Planetary Science Letters*, *515*, 248–259. https://doi.org/10.1016/j.epsl.2019.03.029

Chao, E. C. T., Back, J. M., Minkin, J. A., Tatsumoto, M., Wang, J., Conrad, J. E., et al. (1997). The sedimentary carbonate-hosted giant Bayan Obo REE-Fe-Nb ore deposit of Inner Mongolia, China: A cornerstone example for giant polymetallic ore deposits of hydrothermal origin. *US Geological Survey Bulletin*, *2143*, 1–65.

Chen, W., Liu, H. Y., Lu, J., Jiang, S. Y., Simonetti, A., Xu, C., & Zhang, W. (2020). The formation of the ore-bearing dolomite marble from the giant Bayan Obo REE-Nb-Fe deposit, Inner Mongolia: Insights from micron-scale geochemical data. *Mineralium Deposita*, *55*(1), 131–146. https://doi.org/10.1007/s00126-019-00886-4

Cherniak, D. J., Watson, E. B., Grove, M., & Harrison, T. M. (2004). Pb diffusion in monazite: A combined RBS/SIMS study. *Geochimica et Cosmochimica Acta*, *68*(4), 829–840. https://doi.org/10.1016/j.gca.2003.07.012

Chew, D. M., & Spikings, R. A. (2015). Geochronology and thermochronology using apatite: Time and temperature, lower crust to surface. *Elements*, *11*(3), 189–194. https://doi.org/10.2113/gselements.11.3.189

Cope, T. (2017). Phanerozoic magmatic tempos of North China. *Earth and Planetary Science Letters*, *468*, 1–10. https://doi.org/10.1016/j.epsl.2017.03.022

Copeland, P., Parrish, R. R., & Harrison, T. M. (1988). Identification of inherited radiogenic Pb in monazite and implications for U-Pb systematics. *Nature*, *333*(6175), 760–763. https://doi.org/10.1038/333760a0

Deming, D. (1994). Fluid flow and heat transport in the upper continental crust. In J. Parnell (Ed.), *Geofluids: Origin, migration and evolution of fluids in sedimentary basins* (Vol. 78, pp. 27–42). Geological Society Special Publication.

Deng, M., Xu, C., Song, W., Tang, H., Yun, L., Zhang, Q., et al. (2017). REE mineralization in the Bayan Obo deposit, China: Evidence from mineral paragenesis. *Ore Geology Reviews*, *91*, 100–109. https://doi.org/10.1016/j.oregeorev.2017.10.018

De Yoreo, J. J., Lux, D. R., & Guidotti, C. V. (1991). Thermal modeling in low-pressure/high-temperature metamorphic belts. *Tectonophysics*, *188*(3–4), 209–238. https://doi.org/10.1016/0040-1951(91)90457-4

Fan, H. R., Hu, F. F., Yang, K. F., Wang, K. Y., & Liu, Y. S. (2009). Geochronology framework of late Paleozoic dioritic-granitic plutons in the Bayan Obo area, Inner Mongolia, and tectonic significance. *Acta Petrologica Sinica*, *25*, 2933–2938. (in Chinese with English abstract).

Fan, H. R., Xie, Y. H., Wang, K. Y., Tao, K. J., & Wilde, S. A. (2004). REE daughter minerals trapped in fluid inclusions in the giant Bayan Obo REE-Nb-Fe deposit, Inner Mongolia, China. *International Geology Review*, *46*(7), 638–645. https://doi.org/10.2747/0020-6814.46.7.638

Fan, H. R., Yang, K. F., Hu, F. F., Liu, S., & Wang, K. Y. (2016). The giant Bayan Obo REE-Nb-Fe deposit, China: Controversy and ore genesis. *Geoscience Frontiers*, *7*(3), 335–344. https://doi.org/10.1016/j.gsf.2015.11.005

Gehrels, G., Kronenberg, A., Wernicke, B., Whipple, K., & Wong, T. F. (2003). Geochronology and thermochronology. In *New departures in structural Geology and tectonics: A white paper resulting from a workshop held at Denver Colorado, September 22nd and 23rd, 2002 sponsored by the Tectonics Program* (pp. 49–51). Earth Sciences Division, and National Science Foundation (GEO/EAR).

Gysi, A. P., & Williams-Jones, A. E. (2015). The thermodynamic properties of bastnäsite-(Ce) and parisite-(Ce). *Chemical Geology*, *392*, 87–101. https://doi.org/10.1016/j.chemgeo.2014.11.001

Hodges, K. V. (2014). Thermochronology in orogenic systems. In H. D. Holland & K. K. Turekian (Eds.), *Treatise on geochemistry* (2nd ed., pp. 281–308). Elsevier.

Holland, T., & Blundy, J. (1994). Non-ideal interactions in calcic amphiboles and their bearing on amphibole-plagioclase thermometry. *Contributions to Mineralogy and Petrology*, *116*(4), 433–447. https://doi.org/10.1007/bf00310910

Jagoutz, O. (2014). Arc crustal differentiation mechanisms. *Earth and Planetary Science Letters*, *396*, 267–277. https://doi.org/10.1016/j.epsl.2014.03.060

Jagoutz, O., Schmidt, M. W., Enggist, A., Burg, J. P., Hamid, D., & Hussain, S. (2013). TTG-type plutonic rocks formed in a modern arc batholith by hydrous fractionation in the lower arc crust. *Contributions to Mineralogy and Petrology*, *166*(4), 1099–1118. https://doi.org/10.1007/s00410-013-0911-4

Janka, O., & Schleid, T. (2009). Facile synthesis of Bastnaesite-type $LaF(CO_3)$ and its thermal decomposition to LaOF for bulk and Eu^{3+}-doped samples. *European Journal of Inorganic Chemistry*, *2009*(3), 357–362. https://doi.org/10.1002/ejic.200800931

Jia, H. Y., Xu, L. Q., Zhang, Y. Q., Shang, H. S., Han, J. G., Baoyin, W. L. J., & Luo, Z. Z. (2003). *1:250,000 geological map and explanatory note of Bayan Obo, K49C003002*. National Geological Archive. (in Chinese). https://doi.org/10.35080/n01.c.97979

Jian, P., Kröner, A., Windley, B. F., Zhang, Q., Zhang, W., & Zhang, L. (2012). Episodic mantle melting-crustal reworking in the late Neoarchean of the northwestern North China Craton: Zircon ages of magmatic and metamorphic rocks from the Yinshan Block. *Precambrian Research*, *222–223*, 230–254. https://doi.org/10.1016/j.precamres.2012.03.002

Johnson, M. C., & Rutherford, M. J. (1989). Experimental calibration of the aluminum-in-hornblende geobarometer with application to Long Valley Caldera (California) volcanic rocks. *Geology*, *17*(9), 837–841. https://doi.org/10.1130/0091-7613(1989)017<0837:ecotai>2.3.co;2

Leake, B. E., Woolley, A. R., Arps, C. E. S., Birch, W. D., Gilbert, M. C., Grice, J. D., et al. (1997). Nomenclature of amphiboles: Report of the Subcommittee on amphiboles of the International Mineralogical Association Commission on new minerals and mineral names. *The Canadian Mineralogist*, *35*(405), 219–246. https://doi.org/10.1180/minmag.1997.061.405.13

Le Bas, M. J., Xueming, Y., Taylor, R. N., Spiro, B., Milton, J. A., & Peishan, Z. (2007). New evidence from a calcite-dolomite carbonatite dyke for the magmatic origin of the massive Bayan Obo ore-bearing dolomite marble, Inner Mongolia, China. *Mineralogy and Petrology*, *90*(3–4), 223–248. https://doi.org/10.1007/s00710-006-0177-x

Li, Q., Liu, Y., Tang, G., Wang, K., Ling, X., & Li, J. (2018). Zircon Th–Pb dating by secondary ion mass spectrometry. *Journal of Analytical Atomic Spectrometry*, *33*(9), 1536–1544. https://doi.org/10.1039/c8ja00125a

Li, X., Liu, Y. G., Song, H. P., Zhang, Q., & Wu, X. (2020). Thermal stability and compressibility of bastnaesite. *Physics and Chemistry of Minerals*, *47*(3), 13. https://doi.org/10.1007/s00269-020-01084-9

Li, X.-C., Yang, K.-F., Spandler, C., Fan, H.-R., Zhou, M.-F., Hao, J.-L., & Yang, Y.-H. (2021). The effect of fluid-aided modification on the Sm-Nd and Th-Pb geochronology of monazite and bastnäsite: Implication for resolving complex isotopic age data in REE ore systems. *Geochimica et Cosmochimica Acta*, *300*, 1–24. https://doi.org/10.1016/j.gca.2021.02.028

Li, X.-C., Zhan, Y. X., Fan, H. R., & Yang, K. F. (2022). The REE mineralization and remobilization history of the giant Bayan Obo deposit, Inner Mongolia, China: Constraint from in-situ Sm-Nd isotopes of REE minerals. *Acta Petrologica Sinica*, *38*(10), 2920–2932. (in Chinese with English abstract). https://doi.org/10.18654/1000-0569/2022.10.02

Ling, M. X., Liu, Y. L., Williams, I. S., Teng, F. Z., Yang, X. Y., Ding, X., et al. (2013). Formation of the world's largest REE deposit through protracted fluxing of carbonatite by subduction-derived fluids. *Scientific Reports*, *3*, 1–8. https://doi.org/10.1038/srep01776

Ling, M. X., Zhang, H., Li, H., Liu, Y. L., Liu, J., Li, L. Q., et al. (2014). The Permian–Triassic granitoids in Bayan Obo, North China Craton: A geochemical and geochronological study. *Lithos*, *190–191*, 430–439. https://doi.org/10.1016/j.lithos.2014.01.002

Liu, S., Fan, H. R., Yang, K. F., Hu, F. F., Wang, K. Y., Chen, F. K., et al. (2018). Mesoproterozoic and Paleozoic hydrothermal metasomatism in the giant Bayan Obo REE-Nb-Fe deposit: Constrains from trace elements and Sr-Nd isotope of fluorite and preliminary thermodynamic calculation. *Precambrian Research*, *311*, 228–246. https://doi.org/10.1016/j.precamres.2018.04.021

Liu, S., Wang, C., Liu, D., Wang, J., Ke, C., You, C., & Zhou, B. (2022). REE geochemical characteristics of associated fluorite deposit in the west mine of Bayan Obo and its indicative significance. *Acta Petrologica et Mineralogica*, *41*(5), 903–915. (in Chinese with English abstract).

Liu, Z. H., Xu, Z. Y., Peng, X. D., Yang, Z. S., Liu, M. X., Zhao, D., et al. (2003). *1:250,000 geological map and explanatory note of Baotou, K49C004002*. National Geological Archive. (in Chinese). https://doi.org/10.35080/n01.c.122694

McDougall, I., & Harrision, T. M. (1999). *Geochronology and Thermochronology by the $^{40}Ar/^{39}Ar$ method* (2nd ed., pp. 1–282). Oxford University Press.

McGlashan, N., Brown, L., & Kay, S. (2008). Crustal thickness in the central Andes from teleseismically recorded depth phase precursors. *Geophysical Journal International*, *175*(3), 1013–1022. https://doi.org/10.1111/j.1365-246x.2008.03897.x

McLaren, S., Neumann, N., Sandiford, M., & Wyborn, L. (1999). Post-intrusion heating associated with high-heat-producing Proterozoic granites—Implications for mineralisation? *AGSO Research Newsletter*, (Vol. 30, pp. 23–26). Australian Geological Survey Organization.

McLaren, S., & Powell, R. (2014). Magmatism, orogeny and the origin of high-heat-producing granites in Australian Proterozoic terranes. *Journal of the Geological Society*, *171*, 149–152. https://doi.org/10.1144/jgs2013-040

McLaren, S., Sandiford, M., Dunlap, W. J., Scrimgeour, I., Close, D., & Edgoose, C. (2009). Distribution of palaeozoic reworking in the Western Arunta region and northwestern Amadeus basin from $^{40}Ar/^{39}Ar$ thermochronology: Implications for the evolution of intracratonic basins. *Basin Research*, *21*(3), 315–334. https://doi.org/10.1111/j.1365-2117.2008.00385.x

McLaren, S., Sandiford, M., & Hand, M. (1999). High radiogenic heat–producing granites and metamorphism—An example from the Western Mount Isa inlier, Australia. *Geology*, *27*(8), 679–682. https://doi.org/10.1130/0091-7613(1999)027<0679:hrhpga>2.3.co;2

McLaren, S., Sandiford, M., Hand, M., Neumann, L., & Bastrakova, I. (2003). The hot southern continent: Heat flow and heat-production in Australian Proterozoic terranes. In R. R. Hillis & R. D. Müller (Eds.), *Evolution and dynamics of the Australian plate* (Vol. 372, pp. 157–167). Geological Society of America, Special Papers.

McLaren, S., Sandiford, M., & Powell, R. (2005). Contrasting styles of Proterozoic crustal evolution: A hot-plate tectonic model for Australian terranes. *Geology*, *33*(8), 673–676. https://doi.org/10.1130/g21544ar.1

Mutch, ·E. J. F., Blundy, J. D., Tattitch, B. C., Cooper, F. J., & Brooker, R. A. (2016). An experimental study of amphibole stability in low-pressure granitic magmas and a revised Al-in-hornblende geobarometer. *Contributions to Mineralogy and Petrology*, *171*(10), 85. https://doi.org/10.1007/s00410-016-1298-9

Nadin, E. S., Saleeby, J., & Wong, M. (2016). Thermal evolution of the Sierra Nevada batholith, California, and implications for strain localization. *Geosphere*, *12*(2), 377–399. https://doi.org/10.1130/ges01224.1

Noury, M., Philippon, M., Cornee, J.-J., Bernet, M., Bruguier, O., Montheil, L., et al. (2021). Evolution of a shallow volcanic arc pluton during arc migration: A tectono-thermal integrated study of the St. Martin granodiorites (northern lesser Antilles). *Geochemistry, Geophysics, Geosystems*, *22*(12), e2020GC009627. https://doi.org/10.1029/2020gc009627

Parrish, R. R. (1990). U–Pb dating of monazite and its application to geological problems. *Canadian Journal of Earth Sciences*, *27*(11), 1431–1450. https://doi.org/10.1139/e90-152

Rothstein, D. A., & Manning, C. E. (2003). Geothermal gradients in continental magmatic arcs: Constraints from the eastern peninsular ranges batholith, Baja California, México. In S. E. Johnson, S. R. Paterson, J. M. Fletcher, G. H. Girty, D. L. Kimbrough, & A. Martín-Barajas (Eds.), *Tectonic evolution of northwestern México and the southwestern USA* (Vol. 374, pp. 337–354). Geological Society of America Special Paper.

Saleeby, J., Farley, K. A., Kistler, R. W., & Fleck, R. (2007). Thermal evolution and exhumation of deep-level batholithic exposures, southernmost Sierra Nevada, California. In M. Cloos, W. D. Carlson, M. C. Gilbert, J. G. Liou, & S. S. Sorensen (Eds.), *Convergent margin terranes and associated regions: A tribute to W.G. Ernst* (Vol. 419, pp. 39–66). Geological Society of America Special Paper.

Saltus, R. W., & Lachenbruch, A. H. (1991). Thermal evolution of the Sierra Nevada: Tectonic implications of new heat flow data. *Tectonics*, *10*(2), 325–344. https://doi.org/10.1029/90tc02681

Sandiford, M., McLaren, S., & Neumann, N. (2002). Long-term thermal consequences of the redistribution of heat-producing elements associated with large-scale granitic complexes. *Journal of Metamorphic Geology*, *20*(1), 87–98. https://doi.org/10.1046/j.0263-4929.2001.00359.x

Schmidt, M. W. (1992). Amphibole composition in tonalite as a function of pressure: An experimental calibration of the Al-in-hornblende barometer. *Contributions to Mineralogy and Petrology*, *110*(2–3), 304–310. https://doi.org/10.1007/bf00310745

Schwarz, W. H., & Lippolt, H. J. (2014). ^{40}Ar-^{39}Ar step-heating of impact glasses from the nördlinger Ries impact crater—Implications on excess argon in impact melts and tektites. *Meteoritics & Planetary Sciences*, *49*(6), 1023–1036. https://doi.org/10.1111/maps.12309

Seydoux-Guillaume, A. M., Montel, J. M., Bingen, B., Bosse, V., de Parseval, P., Paquette, J. L., et al. (2012). Low temperature alteration of monazite: Fluid mediated coupled dissolution–precipitation, irradiation damage, and disturbance of the U-Pb and Th-Pb chronometers. *Chemical Geology*, *330–331*, 140–158. https://doi.org/10.1016/j.chemgeo.2012.07.031

Shimazaki, H., Miyawaki, R., Yokoyama, K., Matsubara, S., Yang, Z., & Matsubara, S. (2008). Zhangpeishanite, BaFCl, a new mineral in fluorite from Bayan Obo, Inner Mongolia, China. *European Journal of Mineralogy*, *20*(6), 1141–1144. https://doi.org/10.1127/0935-1221/2009/0021-1888

Slezak, P., & Spandler, C. (2019). Carbonatites as recorders of mantle-derived magmatism and subsequent tectonic events: An example of the Gifford Creek Carbonatite Complex, Western Australia. *Lithos*, *328–329*, 212–227. https://doi.org/10.1016/j.lithos.2019.01.028

Slezak, P., Spandler, C., Border, A., & Whittock, K. (2020). Geology and ore genesis of the carbonatite-associated Yangibana REE district, Gascoyne Province, Western Australia. *Mineralium Deposita*, *56*(5), 1007–1026. https://doi.org/10.1007/s00126-020-01026-z

Smith, M. P., Campbell, L. S., & Kynicky, J. (2015). A review of the genesis of the world class Bayan Obo Fe-REE-Nb deposits, Inner Mongolia, China: Multistage processes and outstanding questions. *Ore Geology Reviews*, *64*, 459–476. https://doi.org/10.1016/j.oregeorev.2014.03.007

Song, W. L., Xu, C., Smith, M. P., Chakhmouradian, A. R., Brenna, M., Kynický, J., et al. (2018). Genesis of the world's largest rare Earth element deposit, Bayan Obo, China: Protracted mineralization evolution over ~1 b.y. *Geology*, *46*(4), 323–326. https://doi.org/10.1130/g39801.1

Stein, E., & Dietl, C. (2001). Hornblende thermobarometry of granitoids from the Central Odenwald (Germany) and their implications for the geotectonic development of the Odenwald. *Mineralogy and Petrology*, *72*(1–3), 185–207. https://doi.org/10.1007/s007100170033

Teufel, S., & Heinrich, W. (1997). Partial resetting of the U–Pb isotope system in monazite through hydrothermal experiments: An SEM and U–Pb isotope study. *Chemical Geology*, *137*(3–4), 273–281. https://doi.org/10.1016/s0009-2541(96)00161-1

Townsend, K. J., Miller, C. F., D'Andrea, J. L., Ayers, J. C., Harrison, T. M., & Coath, C. D. (2000). Low temperature replacement of monazite in the Ireteba granite, southern Nevada: Geochronological implications. *Chemical Geology*, *172*(1–2), 95–112. https://doi.org/10.1016/s0009-2541(00)00238-2

Wei, C., Deng, M., Xu, C., Chakhmouradian, A. R., Smith, M. P., Kynický, J., et al. (2022). Mineralization of the Bayan Obo rare Earth element deposit by recrystallization and decarbonation. *Economic Geology*, *117*(6), 1327–1338. https://doi.org/10.5382/econgeo.4926

Wickham, S. M. (1987). Crustal anatexis and granite petrogenesis during low-pressure regional metamorphism: The Trois Seigneurs Massif, Pyrenees, France. *Journal of Petrology*, *28*(1), 127–169. https://doi.org/10.1093/petrology/28.1.127

Williams, M. L., Jercinovic, M. J., Harlov, D. E., Budzy, B., & Hetherington, C. J. (2011). Resetting monazite ages during fluid-related alteration. *Chemical Geology*, *283*(3–4), 218–225. https://doi.org/10.1016/j.chemgeo.2011.01.019

Wilson, M. R., & Åkerblom, G. V. (1982). Geological setting and geochemistry of uranium-rich granites in the Proterozoic of Sweden. *Mineralogical Magazine*, *46*(339), 233–245. https://doi.org/10.1180/minmag.1982.046.339.10

Wu, F., Zhang, S., Zhao, Y., & Ye, H. (2014). Emplacement depths of the Early Permian plutons in Guyang area of northern North China Block and their tectonic implications. *Geology in China*, *41*(3), 824–837. (in Chinese with English abstract).

Yang, J. H., Wu, F. Y., Wilde, S. A., Belousova, E., & Griffin, W. L. (2008). Mesozoic decratonization of the North China block. *Geology*, *36*(6), 467–470. https://doi.org/10.1130/g24518a.1

Yang, K. F., Fan, H., Pirajno, F., & Li, X. (2019). The Bayan Obo (China) giant REE accumulation conundrum elucidated by intense magmatic differentiation of carbonatite. *Geology*, *47*(12), 1198–1202. https://doi.org/10.1130/g46674.1

Yang, X. Y., Lai, X. D., Franco, P., Liu, Y. L., Ling, M. X., & Sun, W. D. (2017). Genesis of the Bayan Obo Fe-REE-Nb formation in Inner Mongolia, north China craton: A perspective review. *Precambrian Research*, *288*, 39–71. https://doi.org/10.1016/j.precamres.2016.11.008

Yang, Y. H., Wu, F. Y., Li, Q. L., Rojas-Agramonte, Y., Yang, J. H., Li, Y., et al. (2019b). In situ U-Th-Pb dating and Sr-Nd isotope analysis of bastnäsite by LA-(MC)-ICP-MS. *Geostandards and Geoanalytical Research*, *43*(4), 543–565. https://doi.org/10.1111/ggr.12297

Zhang, P. S., & Tao, K. J. (1986). *Bayan Obo mineralogy* (pp. 1–209). Science Press. (in Chinese with English abstract).

Zhang, S. H., & Zhao, Y. (2013). Mid-crustal emplacement and deformation of plutons in an Andean-style continental arc along the northern margin of the North China block and tectonic implications. *Tectonophysics*, *608*, 176–195. https://doi.org/10.1016/j.tecto.2013.09.036

Zhang, S. H., & Zhao, Y. (2017). Cogenetic origin of mafic microgranular enclaves in calc-alkaline granitoids: The Permian plutons in the northern North China Block. *Geosphere*, *13*(2), 482–517. https://doi.org/10.1130/ges01407.1

Zhang, S. H., Zhao, Y., Davis, G. A., Ye, H., & Wu, F. (2014). Temporal and spatial variations of Mesozoic magmatism and deformations in the North China Craton: Implications for lithospheric thinning and decratonization. *Earth-Science Reviews*, *131*, 49–87. https://doi.org/10.1016/j.earscirev.2013.12.004

Zhang, S. H., Zhao, Y., Li, Q. L., Hu, Z. C., & Chen, Z. Y. (2017). First identification of baddeleyite related/linked to contact metamorphism from carbonatites in the world's largest REE deposit, Bayan Obo in North China Craton. *Lithos*, *284–285*, 654–665. https://doi.org/10.1016/j.lithos.2017.05.015

Zhang, S. H., Zhao, Y., Liu, J. M., & Hu, Z. C. (2016). Different sources involved in generation of continental arc volcanism: The Carboniferous-Permian volcanic rocks in the northern margin of the North China block. *Lithos*, *240–243*, 382–401. https://doi.org/10.1016/j.lithos.2015.11.027

Zhang, S. H., Zhao, Y., & Liu, Y. (2017). A precise zircon Th-Pb age of carbonatite sills from the world's largest Bayan Obo deposit: Implications for timing and genesis of REE-Nb mineralization. *Precambrian Research*, *291*, 202–219. https://doi.org/10.1016/j.precamres.2017.01.024

Zhang, S. H., Zhao, Y., Pei, J. L., Zhang, Q. Q., Miggins, D. P., & Koppers, A. A. P. (2019). Paleogeotherms of a midcrustal to upper-crustal profile across the northern North China Block: Implications for the thermal structure of continental arcs. *Tectonics*, *38*(2), 706–721. https://doi.org/10.1029/2018tc005154

Zhang, S. H., Zhao, Y., Song, B., Hu, J. M., Liu, S. W., Yang, Y. H., et al. (2009). Contrasting late Carboniferous and late Permian-middle Triassic intrusive suites from the northern margin of the North China craton: Geochronology, petrogenesis and tectonic implications. *Geological Society of America Bulletin*, *121*(1−2), 181–200. https://doi.org/10.1130/b26157.1

Zhang, S. H., Zhao, Y., Song, B., Yang, Z. Y., Hu, J. M., & Wu, H. (2007). Carboniferous granitic plutons from the northern margin of the North China block: Implications for a Late Paleozoic active continental margin. *Journal of the Geological Society London*, *164*(2), 451–463. https://doi.org/10.1144/0016-76492005-190

Zhang, S. H., Zhao, Y., Ye, H., Liu, J. M., & Hu, Z. C. (2014). Origin and evolution of the Bainaimiao arc belt: Implications for crustal growth in the southern central Asian orogenic belt. *Geological Society of America Bulletin*, *126*(9–10), 1275–1300. https://doi.org/10.1130/b31042.1

Zhang, W., Chen, W. T., Harlov, D., & Gao, J.-F. (2023). Resetting of the U-Pb and Th-Pb systems in altered bastnäsite: Insight from the behavior of Pb at nano-scale. *American Mineralogist*, *108*(3), 465–475. https://doi.org/10.2138/am-2022-8318

Zhang, X. H., Gao, Y., Wang, Z., Liu, H., & Ma, Y. (2012). Carboniferous appinitic intrusions from the northern North China craton: Geochemistry, petrogenesis and tectonic implications. *Journal of the Geological Society*, *169*(3), 337–351. https://doi.org/10.1144/0016-76492011-062

Zhang, X. H., Yuan, L., Xue, F., & Zhai, M. (2014). Neoarchaean metagabbro and charnockite in the Yinshan block, Western North China Craton: Petrogenesis and tectonic implications. *Precambrian Research*, *255*, 563–582. https://doi.org/10.1016/j.precamres.2013.11.003

Zhao, G. C., Sun, M., Wilde, S. A., & Li, S. Z. (2005). Late Archean to paleoproterozoic evolution of the North China craton: Key issues revisited. *Precambrian Research*, *136*(2), 177–202. https://doi.org/10.1016/j.precamres.2004.10.002

Zhu, X. K., Sun, J., & Pan, C. X. (2015). Sm-Nd isotopic constraints on rare-Earth mineralization in the Bayan Obo ore deposit, Inner Mongolia, China. *Ore Geology Reviews*, *64*, 543–553. https://doi.org/10.1016/j.oregeorev.2014.05.015

Zi, J. W., Gregory, C., Rasmussen, B., Sheppard, S., & Muhling, J. R. (2017). Using monazite geochronology to test the plume model for carbonatites: The example of Gifford Creek carbonatite complex, Australia. *Chemical Geology*, *463*, 50–60. https://doi.org/10.1016/j.chemgeo.2017.05.007

References From the Supporting Information

Chen, W., Zhang, Y., Zhang, Y. Q., Jin, G. S., & Wang, Q. L. (2006). Late Cenozoic episodic uplifting in southeastern part of the Tibetan plateau: Evidence from Ar-Ar thermochronology. *Acta Petrologica Sinica*, *22*, 867–872. (in Chinese with English abstract).

Koppers, A. A. P. (2002). ArArCALC—Software for $^{40}Ar/^{39}Ar$ age calculations. *Computers & Geosciences*, *28*(5), 605–619. https://doi.org/10.1016/s0098-3004(01)00095-4

Koppers, A., Staudigel, H., Wijbrans, J. R., & Pringle, M. (2003). Short-lived and discontinuous intraplate volcanism in the South Pacific: Hot spots or extensional volcanism? *Geochemistry, Geophysics, Geosystems*, *4*(10), 1089. https://doi.org/10.1029/2003GC000533

Koppers, A. A. P., Gowen, M. D., Colwell, L. E., Gee, J. S., Lonsdale, P. F., Mahoney, J. J., & Duncan, R. A. (2011). New $^{40}Ar/^{39}Ar$ age progression for the Louisville hot spot trail and implications for inter–hot spot motion. *Geochemistry, Geophysics, Geosystems*, *12*, Q0AM02. https://doi.org/10.1029/2011GC003804

Kuiper, K. F., Deino, A., Hilgen, F. J., Krijgsman, W., Renne, P. R., & Wijbrans, J. R. (2008). Synchronizing rock clocks of Earth history. *Science*, *320*(5875), 500–504. https://doi.org/10.1126/science.1154339

Liu, Y. S., Hu, Z. C., Zong, K. Q., Gao, C. G., Gao, S., Xu, J., & Chen, H. H. (2010). Reappraisal and refinement of zircon U-Pb isotope and trace element analyses by LA-ICP-MS. *Chinese Science Bulletin*, *55*(15), 1535–1546. https://doi.org/10.1007/s11434-010-3052-4

Ludwig, K. R. (2003). *User's manual for Isoplot 3.00* (p. 70). A geochronological Toolkit for Microsoft Excel: Berkeley Geochronology Center.

Min, K., Mundil, R., Renne, P. R., & Ludwig, K. R. (2000). A test for systematic errors in $^{40}Ar/^{39}Ar$ geochronology through comparison with U/Pb analysis of a 1.1-Ga rhyolite. *Geochimica et Cosmochimica Acta*, *64*(1), 73–98. https://doi.org/10.1016/s0016-7037(99)00204-5

Steiger, R. H., & Jäger, E. (1977). Subcommission on geochronology: Convention on the use of decay constant in geo- and cosmochronology. *Earth and Planetary Science Letters*, *36*(3), 359–362. https://doi.org/10.1016/0012-821x(77)90060-7

Taylor, J. R. (1997). *An introduction to error analysis: The study of uncertainties in physical measurements* (p. 327). University Science Books, Mill Valley, California.

Wang, S., Zhang, S. H., Zhang, Q. Q., Liang, X., Kong, L. H., Hu, G. H., et al. (2022). In-situ zircon U-Pb dating method by LA-ICP-MS and discussions on the effect of different beam spot diameters on the dating results. *Journal of Geomechnics*, *28*(4), 642–652. (in Chinese with English abstract).

York, D. (1969). Least squares fitting of a straight line with correlated errors. *Earth and Planetary Science Letters*, *5*, 320–324. https://doi.org/10.1016/s0012-821x(68)80059-7

Zhang, Y., Chen, W., Chen, K. L., & Liu, X. Y. (2006). Study on the Ar-Ar age spectrum of diagenetic I/S and the mechanism of ^{39}Ar recoil loss: Examples from the clay minerals of P-T boundary in Changxing, Zhejiang Province. *Geological Review*, *52*, 556–561. (in Chinese with English abstract).